Assimilating Data from Incubations into a Multi-element Ecosystem Model

S. Lan Smith

Ecosystem Change Program, Frontier Research System for Global Change, Yokohama, Japan

Beatriz E. Casareto

Laboratory of Aquatic Sciencies Consultant Co., Tokyo, Japan

Mohan P. Niraula and Yoshimi Suzuki

Shizuoka University, Shizuoka, Japan

Julia C. Hargreaves and James D. Annan

Frontier Research System for Global Change, Yokohama, Japan, and Proudman Oceanographic Laboratory, Liverpool, UK

Yasuhiro Yamanaka

Ecosystem Change Program, Frontier Research System for Global Change

Keywords: Model, Assimilation, Stoichiometry, Remineralization, Ecosystem

---

S. Lan Smith, Frontier Research System for Global Change 3173-25 Showa-machi, Kanazawa-ku, Yokohama-shi Kanagawa-ken, Japan 236-0001 (e-mail: lanimal@jamstec.go.jp)

Beatriz E. Casareto, Laboratory of Aquatic Sciences Consultant Co. Tokyo, Japan

Mohan P. Niraula and Yoshimi Suzuki, Global Biogeochemistry Laboratory, Shizuoka University, Shizuoka, Japan

Abstract.

We have developed a new, multi-element ecosystem model to simulate a set of batch incubation experiments of natural phytoplankton assemblages. The model divides organisms into classes based on differences in size and function and simulates the flexible-composition of phytoplankton. Nutrient concentrations and plankton community differed among the incubations, allowing us to examine the functioning of the ecosystem by comparison. Data included concentrations of nutrients, organic matter (particulate and dissolved) and plankton (biomass by species). We used a Monte Carlo Markov Chain method to assimilate these data into our model and examined the distributions of simulated values from the ensemble of simulations. The model simulated well the changes in C:N ratio of bulk particulate organic matter (POM), and its difference between experiments. We examined the simulated gross flows of carbon and nitrogen (which cannot be directly measured), dividing the ecosystem between the Microbial Food Web (MFW) and Grazing Food Web (GFW) based on the size of organisms. The MFW dominated the flow of nitrogen in all incubations. The bulk POC:PON ratio varied inversely with the gross amount of nitrogen remineralized in a given incubation. The flexible composition of phytoplankton is a key link between remineralization and the dynamic stoichiometry of POM.

INTRODUCTION

Marine ecosystem models are now widely applied for simulating biogeochemical cycles. Most studies use estimates of rates and other parameters from various studies and adjust parameters to fit the model to available data. Sensitivity analysis often aids this process, but few studies have applied mathematically rigorous methods to assimiliate data into ecosystem models. Vallino (Vallino, 2000) assimilated data from mesocosm experiments into an ecosystem model and demonstrated the use of a "modeling workbench" for model development (using assimilation to quantitatively compare models). Other studies have assimilated data from time-series observations. Spitz *et al* (Spitz *et al*, 2001) assimilated data from the Bermuda Atlantic Time Series (BATS) site into an ecosystem model coupled to a one dimensional physical model and used the assimilations to guide model improvements. Schartau *et al* (Schartau *et al*, 2001) assimilated data from BATS into a zero-dimensional model. Friedrichs (Friedrichs, 2001) assimilated data from the Joint Global Ocean Flux Study (JGOFS) Equatorial Pacific Process Study (EqPac) and satelite data into an ecosystem model. Harmon and Challenor (Harmon and Challenor, 1997) demonstrated the potential of the Monte Carlo Markov Chain method for estimating the parameters of a simple ecosystem model, but it has not to our knowledge been tested in an application with real ecosystem data.

METHOD

We have assimilated data from a set of incubation experiments into a new multi-element ecosystem model designed specifically to simulate these experiments. In the experiments, seawater from three depths (Surface, 400m and 700m) from Suruga Bay, Japan, was incubated in 30 liter bottles, under attenuated natural surface irradiation in a water bath to control temperature. Niraula *et al* (submitted jointly) describe the experiments in detail. By comparing the incubations using water from different depths, they examined the dynamics of the ecosystem under different conditions.

We sought to examine flows through the ecosystem which cannot be directly measured. The primary motivation for this was to test a hypothesis based on these experiments, namely that it is the phytoplankton species composition that determines the relative importance of the microbial food web (MFW) versus the grazing food web (GFW). Their relative roles are important for understanding marine biogeochemistry in the upper ocean, because the MFW regenerates nutrients and carbon, whereas the GFW produces larger particles which are expected to export nutrients and carbon from the upper ocean.

We also sought to constrain parameters for the model, using both chemical and biological data from these mesocosm incubations. Aggregatated models (which simulate functional classes of organisms instead of species) like ours often do not yield the best simulations using parameters based on culture

experiments or allometric relationships (Vallino, 2000). Our data set suits this study well because of the high temporal resolution of observations (usually at 2 day intervals) and the nearly simultaneous measurements of various biological and chemical quantities in natural seawater.

Data: The experiments and data are described by Niraula *et al* (submitted jointly). Measurements of nutrients included nitrate, nitrite, ammonium, silicic acid and phosphate. Dissolved organic carbon (DOC) and nitrogen (DON) and partriculate organic carbon (POC) and nitrogen (PON) were measured. Particulate silica (PSi) was also measured. From cell counts and biovolumes (calculated from observed dimensions), biomasses were estimated for phytoplankton and zooplankton by species, and for bacteria and nanoflagellates. Irradiation and temperature were measured continuously within the water bath containing the incubation bottles.

Model: Figure 1 shows a diagram of the ecosystem model and table I lists its compartments. The model includes compartments for three classes of phytoplankton: non-silicious phytoplankton (*PhyS*), and small and large diatoms (*DiaS* and *DiaL*, respectively). For each of these, the carbon, nitrogen and chlorophyll concentrations are simulated separately, according to the model by Geider *et al* (Geider *et al*, 1998). Three heterotrophic compartments are included: bacteria (*B*), heterotrophic nanoflagellates (*HNF*), and zooplankton (*Z*). Only the nitrogen concentrations of heterotrophs are simulated, and fixed stoichiometries are assumed for each. Trophic relationships are determined according to the size of organisms (see appendix). Three compartments are included for the carbon, nitrogen and phosphorus in dissolved organic matter (*DOM*), and three more for particulate organic matter (*POM*). The model also simulates nitrate (NO_3), ammonium (NH_4), phosphate (PO_4), silicic acid (*DSi*), and biogenic silica (*BSi*). The appendix describes the model in detail, and tables II and III list parameters.

Parameters: Some changes were made to the phytoplankton model (Geider *et al*, 1998) to embed it into our ecosystem model. The original model, applied to culture experiments, assumed no mortality, and set the respiration rates to zero. We have set the respiration rate coefficient at 0.10 day^{-1} from a study simulating ocean station BATS with a similar phytoplankton model (Lefevre *et al*, 2003). This means that our model should require higher rates of photosynthesis than the original model, to balance respiration and mortality. We set an initial guess for the maximum rates of photosynthesis and let them vary in the assimilation. We set mortality rates to those of Fujii *et al* (Fujii *et al*, 2002a), which were used in simulations of several ocean time series sites. All other parameters for phytoplankton are from the original phytoplankton model (Geider *et al*, 1998), or from Fujii *et al* (Fujii *et al*, 2002a). Parameters for bacteria and DOM are from Anderson and Williams (Anderson and Williams, 1998), or are based on their values. We simplified their model to use first-order kinetics for DOM degradation (because concentrations are never high enough to approach saturation with the high half-saturation

concentrations in their model) and to include only one class of (non-refractory) DOM. Therefore, the rate we applied for DOM degradation is their rate for semi-labile DOM degradation, divided by their half-saturation coefficient for uptake of semi-labile DOM. For heterotrophic nanoflagellates, we applied a growth efficiency of 0.50 (Goldman and Caron, 1985). For zooplankton (primarily ciliates), we applied a value 0.50 (Verity, 1992). For POM degradation, we used the first-order rate reported for non-refractory POM by Fujii *et al* (Fujii *et al*, 2002b) based on their decompositon experiments (neglecting the small refractory fraction of POM found in that study).

Initialization and Solution: The simulation was begun on the second day for each incubation, because of the very low initial biomasses (some below detection limits) and because of the difficulty of simulating the lag phase at the beginning of the experiment, as found in other studies (Geider *et al*, 1998). Nutrients and carbon biomasses for phytoplankton were initialized to the observed values. Initial nitrogen and chlorophyll for phytoplankton were calculated assuming a C:N ratio of 6.6 and a Chl:N ratio of 0.15 (g Chl/ g N), which was half the maximum value from the original model (Geider *et al*, 1998). Nitrogen biomasses for bacteria and zooplankton were set based on the observed carbon biomasses and the C:N ratios of each organism-compartment (table III). Detritus (POC and PON) concentrations were initialized to the observed POM concentrations minus the sum of all POM in organism-compartments, and POP was set assuming an N:P ratio of 16 (the Redfield ratio). DOC and DON were initialized to observed values, and DOP was set assuming an N:P ratio of 16. Observed irradiance and temperature were used to drive the model. The timestep was one minute. We verified that the model conserved mass of nitrogen, carbon and phosphorus.

Assimilation Method: We applied the Monte Carlo Markov Chain method as applied by Harmon and Challoner (Harmon and Challoner, 1997) and Hargreaves and Annan (Hargreaves and Annan, 2002). This method performs a random walk through parameter space by iterating the following procedure: generate a trial set of parameters by randomly perturbing the current parameter set, run a simulation with the trial set of parameters, calculate a "cost" for that simulation based on the difference between model and data, and decide whether to step to the trial parameter set (based solely on a comparison of this cost with that of the current parameter set). A step to a better parameter set (lower cost) is always taken, and a step to a worse one is sometimes taken based on a randomised decision which depends on how much worse the simulation is. This allows the method to proceed towards better simulations and avoid local minima. After running the walk to (statistical) convergence, the resulting ensemble of runs samples the joint posterior probability distribution function defined by the data.

To calculate the cost function for each data type, *i*, we use the common approach of using the reciprocal of the estimated standard deviation of measurement, σ_i, as a weight, except as discussed below for *POM*. The total cost is then:

$$Cost = \sum_i \left(\frac{C_i^{sim} - C_i^{obs}}{\sigma_i} \right)^2 \quad (1)$$

In which C_i^{sim} is the simulated value corresponding to observed value C_i^{obs}, and the sum covers all data points of each type. σ was 0.05 μM for PO_4. σ's were 0.10 μM for NO_3, NH_4, *POC* and *PON* and for the biomasses of bacteria (*BactC*), small phytoplankton (*PhySC*) and heterotrophic nanoflagellates (*HNFC*). They were 1.0 μM for the biomasses of small diatoms (*DiaSC*) and zooplankton (*ZC*), 0.3 μM for *DON*, 1.0 μM for *DOC*, and 2.0 μM for the biomass of large diatoms (*DiaLC*).

For *POM*, however, the weighting was adjusted to account for a problem with the measuremts. Figure 2 shows a mass balance of nitrogen (sums of *DON*, *PON* and dissolved inorganic nitrogen,*DIN*), together with independent measurements of total nitrogen, over time for each of the three incubations. The total amount of nitrogen observed was lowest in the middle of each experiment. A balance for silicon (not shown) reveals a similar pattern, and the imbalance as a fraction of drawdown is slightly greater for silicon. This suggests that the problem is with the *POM* measurements rather than with the *DOM* measurements, because for silicon there is no pool corresponding to *DON*. We therefore took the observed POM concentrations as lower bounds, and only added their terms to the cost function when the model underestimated them. To compensate for the lack of an upper bound on POC and PON, a cost was added for the bulk POC:PON ratio, using $\sigma_{RPOM} = \sigma_{POC}/PON$ (using the observed *PON* concentration at each sampling time). Thus, information from the stoichiometry of POM could be incorporated into the assimilation, despite the mass imbalance in the data (assuming that the observed POC:PON ratio is correct despite the mass imbalance).

To widen the distributions of simulated values, all weights for each incubation were divided by a factor of 20 (allowing acceptance of more parameter sets).

Parameters optimised: Because we sought to compare the MFW and GFW, we strove for balance in choosing which parameters to vary. It would not make sense to vary only (or mostly) parameters of the MFW and then to compare the two food webs in the resulting simulations. We varied the maximum rate of photosynthesis and the fraction of production as DOM, separately for each phytoplankton class. For bacteria, the maximum uptake rate of DOM was varied. For both heterotrophic nanoflagellates and zooplankton, a single, distinct grazing rate was assumed to apply for all prey. Thus two grazing rates were varied. Tables IV, V and VI list the parameters varied in each assimilation, except for

the perturbations to initial conditions of organisms. In addition to the parameters listed separately, a variable perturbation (values not shown) was introduced for the initial concentration of each of the (six) organism compartments. The absolute value of each perturbation was limited to be within one standard deviation of measurement for the biomass and to be greater than whatever negative value would yield an intial concentration of zero for each compartment. A total of 15 parameters were varied in each assimilation.

For each parameter a scaling factor was used to fix the maximum absolute value of the perturbation for each run in the assimilation. The scaling factors were 0.0045 for μ_B and 0.06 for both grazing rates. All other parameter were restricted to a fixed range; any parameter set in which one parameter exceeded its range was rejected without running a simulation. The fractions of production as DOM for each phytoplankton (γ's) were restricted to a (0,1) range, with a scaling factor of 0.03. For the perturbations to initial conditions a range of (0,1) and a scaling factor of 0.03 were applied, and the resulting variables were rescaled to (-1,1) variables and multiplied by the perturbation range for each species.

Previous assimilations were run without an upper bound on either the rates of photosynthesis or grazing (not shown). These resulted in a wide range of values for both rates of photosysnthesis and grazing, with some values continuing to increase throughout the assimilation. The assimilation cannot constrain both sets of rates with the available data. We therefore decided to seek the lowest rates of photosysnthesis and grazing that yielded simulations consistent with the data. The rates of photosynthesis were limited to a range between zero and a maximum value, by multiplying the (0,1) variable by this maximum value. A scaling factor of 0.06 was used for varying the (0,1) variables. By trial and error, we found that a maximum value of 15 day^{-1} allowed consistent simulations.

RESULTS

For the following analysis the final ensemble of runs for each assimilation was constructed by taking every 5000th run from the second half of the MCMC. The second half was used in order to make sure that the MCMC had converged. Verification of this choice is demonstrated in Figure 3, the upper plots of which show the variation of parameter μ_B (bacterial uptake rate) with run number for each assimilation. This parameter clearly converges within the first half of the model runs for all three assimilations. The lower plots, showing the variation of the cost with model run number, indicate a similar convergence for the model as a whole.

Table IV lists the parameters varied in the assimilation for the Surface Incubation, except for the perturbations to initial conditions for organism (which are not shown). Table IV also lists the best-fit, median and inter-quantile range (from 5 % quantile to 95 % quantile)of the final ensemble for each

parameter listed. Quantiles are from a sampling of the accepted parameter sets, sampled every 5000 sets (from the latter half of the assimilation). Tables V and VI list the same values for the assimilations of the 400m and 700m incubations, respectively.

The percentages of parameter sets accepted were 78 %, 0.13 % and 0.31 % respectively for the Surface, 400m and 700m assimilations. In the 400m and 700m assimilations many parameter sets were rejected without running simulations, because parameters exceeded their bounds. This happened because several parameters (most importantly P^{ref}_{DiaS}, γ_{DiaS} and γ_{DiaL}) were constrained to values close to their bounds (Tables V and VI). A total of 1.4 million parameter sets were tried for the Surface assimilation, 8.9 million for the 400m, and 3.0 million for the 700m. Compared to the Surface case, the 400m and 700m assimilations tried more parameter sets in the same run-time (real time), because many parameter sets were rejected without running simulations.

Figure 3 shows the evolution of the parameter μ_B, bacterial uptake rate, and the total cost for each of the three assimilations. The upper plots illustrate the relative success of the assimilation at the three levels. Mu varies over only a limited range for the deep water incubations, but varies very widely for the surface case. This indicates that the data from the surface water incubation are insufficient to constrain the model well. The next section discusses this problem further.

Figure 4 shows the data and simulations for the Surface incubation, including all assimilated data and that for silicic acid and biogenic silica, which were not assimilated. Quantiles of simulated values are from a sampling of the accepted simulations (every 5000 simulations, as for parameters). In this figure, the simulated POC and PON are the bulk quantities (including detritus and biomasses of all organisms). Figures 5 and 6 show the corresponding data and simulations for the 400m and 700m incubations, respectively.

Figure 7 presents the simulated and observed POC:PON ratios for all three incubations.

Figure 8 shows the simulated gross uptake and gross remineralization of carbon, and the net uptake (the sum of uptake and remineralization, or the storage of carbon as organic matter). Data shown are the total organic carbon, TOC (= DOC + POC) measured (subtracting the value at the start of each simulation). Because of the problem with the mass balance of nitrogen (discussed above), we expect that the observed POC values are too low. Based on this and the lower penalty assigned to overestimates of POC in the assimilation (discussed above), we would expect the model to underestimate net carbon uptake. However, the incorrect stoichiometry for DOM in the model counteracts this effect. The model tends to underestimate the storage of organic carbon, except for the 700m incubation. Figure 9 shows a similar plot of nitrogen, revealing that the model tends to overestimate storage of organic nitrogen, as expected.

Figure 10 is a diagram of the simulated flows of nitrogen in the best-fit simulation of the 400m incubation. Figure 11 is the same diagram for the 700m case.

Figure 12 shows the uptake (gross production) of nitrogen, divided between the microbial food web (MFW) and grazing food web (GFW). Any organism smaller than 5 μm was counted as part of the MFW, while any larger than 5 μm was counted as part of the GFW. Thus, the MFW included bacteria, small phytoplankton, small diatoms and heterotrophic nanoflagellates. The GFW included large diatoms and zooplankton.

DISCUSSION

The fit to the Surface incubation was the worst of the three, because this incubation had the smallest changes in concentrations and therefore the lowest signal-to-noise ratio. Parameters were not well constrained in the Surface assimilation, as Figure 3 illustrates for μ_B. Parameters were better constrained in the deeper-water incubations, and the ranges of simulated values were narrower (Figures 5 and 6). We therefore concentrate on the 400m and 700m incubations in the following discussion.

Rates of Photosynthesis: The best-fit values for maximum photosysthesis rates were generally much higher than those in the original phytoplankton model, which were either 3.0 or 5.1 day^{-1} (Geider *et al*, 1998). This is because we were simulating batch incubations, starting from very low phytoplankton concentrations. The original model was applied to culture experiments under conditions of balanced growth, meaning that the relative rates of change of phytoplankton C, N and Chl were equal (Geider *et al*, 1998). The original model also ignored respiration (set all respiration rates to zero). Any model that includes non-zero respiration should require higher growth rates to simulate the same data. The rates should then be greater by approximately the value of the respiration rate coefficient (0.10 day^{-1} at 20 °C, in this study). Some of our rates are several times those in the original study. They are also greater than those used by Lefevre *et al* (Lefevre *et al*, 2003) in their study simulating ocean time series, even though we use the same respiration rate coefficient. The faster rates in this study are required to simulate the dynamics of the batch incubations.

As discussed above, we restricted the rates of photosysnthesis, using a maximum value of 15 day^{-1}, because otherwise both rates of photosynthesis and grazing continued to increase throughout the assimilations. Because the assimilation cannot constrain both the photosysnthesis and grazing rates with the available data, we sought the lowest rates consistent with the data. For diatoms in the 400m and 700m incubations, the assimilation prefered rates of photosysnthesis close to the maximum (values and quantile ranges in Tables V and VI). We would need more information (e.g., data for primary production or zooplankton grazing rates) to constrain these rates.

Other parameters: The best-fit and median values of rates for bacterial uptake differed for the 400m and 700m cases (best values were 0.61 and 0.82 day^{-1} (μM N)$^{-1}$, respectively; see Tables V and VI). Grazing rates were very similar. The fraction of production as DOM for both small and large diatoms (γ_{DiaS} and γ_{DiaL}) were low (a few percent or less) for both incubations. Parameters for small phytoplankton, *PhyS*, differed more. These were not as well constrained because small phytoplankton did not constitute a major fraction of the biomass in either incubation.

Phytoplankton biomass: The trends in biomass over time for diatoms are qualitatively well simulated, although the biomasses are overestimated. In both the data and the simulations for the 400m and 700m incubations, biomass of small diatoms peaks early, but biomass of large diatoms is higher at the end. The half-saturation coefficients for uptake were the same for small and large diatoms. The model achieved this qualtative agreement without any difference in nutrient preference for small and large diatoms, consistent with the findings of Niraula *et al* (submitted jointly).

The peak biomass of small diatoms is greatly overestimated for both the 400m and 700m incubations (Figures 5 and 6), and the biomass of large diatoms is also overestimated. This may be because the mortality rates used in the model are too low. The lack of an upper bound for POM (because of the mass balance problem discussed above) makes it easier for the assimilations to find solutions that overestimate these biomasses.

Stoichiometry of POM: Because the ecosystem model includes bacteria and the variable stoichiometry model for phytoplankton, we can compare our simulated bulk POM (detrital POM plus organisms) directly with the observed, bulk POM. Mongin *et al* (Mongin *et al*, 2003) obtained good simulations of the depth profile of bulk POC:PON ratio for station BATS using a similar model. Such a direct comparison is not possible with models that do not include bacteria and detritus (Lefevre *et al*, 2003). In the deeper water incubations (400m and 700m) POC:PON ratios are lower early in the experiment when nutrients are replete. They then increase after nutrients are depleted. The flexible composition phytoplankton model (Geider *et al*, 1998), embedded in the explicit carbon and nitrogen cycles of our model, simulates these trends and the difference between the 400m and 700m incubations (Figure 7).

The phytoplankton model can only produce biomass with high C:N ratios when nitrogen supply is limited. POM stoichiometry therefore constrains nitrogen remineralization in the assimilations. The higher bulk POC:PON ratios in the 400m incubation (Figure 7) limit remineralization more than the lower values for the 700m incubation. Simulated gross remineralization of nitrogen is greater for the 700m case (Figure 9). This is consistent with the observations in the 700m experiment, namely the high bacterial biomass and the early peak of the small diatom *Thalassiosira minima* (Niraula *et al*, submitted jointly), which is known to produce a great deal of DOM (B. Casareto, unpublished data).

We did not vary the minimum or maximum N:C cell quotas, which respectively determine the maximum and minimum possible C:N ratios for phytoplankton. Of course one could try fitting the observed C:N ratios by varying these parameters. Lefevre *et al* (Lefevre *et al*, 2003) varied the minimum cell quota in their sensitivity analysis, but found only moderate changes in the C:N ratio of phytoplankton. This is because in their simulations, as in ours, the phytoplankton do not approach their minimum cell quotas (maximum C:N ratios). They do approach their maximum cell quotas early in both our 400m and 700m simulations, and the bulk C:N ratio is underestimated, most notably in the 400m case (Figure 7). It would probably not be possible to constrain both the flows and the minimum and maximum cell quotas in this study.

Flexible Stoichiometry of Phytoplankton vs. Differential Remineralization: Our model simulated well the POC:PON ratios in these incubation experiments without allowing differential remineralization of C and N. Some recent modeling studies have fixed the stoichiometry of POM to match the high C:N ratios of detritus, while applying Redfield stoichiometry for phytoplankton (Anderson and Williams, 1998; Smith *et al*, 2004), or allowed differential remineralization of carbon and nitrogen (Bisset *et al*, 1999). There is evidence for differential remineralization of carbon and nitrogen between 150m and 500m meters from sediment traps at Stn. ALOHA (Christian *et al*, 1997). Our model does not allow differential remineralization, and we do not know whether or not it occurred in these experiments. If it did, the flexible composition of phytoplankton would have compensated by decreasing the C:N ratio of production (because of the enhanced recycling of N). Although its effect would not be as strong as in this batch system, this compensation would also be expected to regulate POC:PON ratios in the ocean.

Our results suggest that the flexible composition of phytoplankton may account for the high POC:PON ratios in shallow sediment traps without invoking differential remineralization. Although the remineralization of sinking particles over scales of hundreds of meters in the ocean may differ from that in incubation experiments, it is worth examining to what extent phytoplankton compostion alone might explain observed POM stoichiometry. If fixed stoichiometries must be used in large-scale ocean models, we suggest that it makes more sense to fix the stoichiometry of phytoplankton themselves to a higher-than-Redfield value, as did Hood *et al* (Hood *et al*, 2001), than to fix the detrital ratio.

Stoichiometry of DOM: The model underestimates DOC concentrations in both of the deeper-water incubations, and the simulated DOC:DON ratios are too low. The problem with DOM stoichiometry is a fundamental shortcoming of the model. Observed ratios of DOC:DON were higher than those of POC:PON, especially after the first few days of each incubation. Other experiments have found similar results (Vallino, 2001). Our model assumes that phytoplankton excrete DOM with the same

stoichiometry as their biomass, and that other sources and sinks of DOM are determined by mass balance among the various compartments.

In the assimilation, the weights were low for DOC relative to most other compartments in the model, because of its relatively large standard deviation of measurement (1 μM). DON is simulated better, partly because it's lower standard deviation of measurement (0.3 μM) gives it a higher weight. Still, the fraction of production as DOM for small diatoms (γ_{DiaS}) should be relatively high in both the 400m and 700m cases, given the presence of *Thalassiosira minima*, which is known to produce a great deal of DOM. This should be true especially in the 700m case, because this species dominated the initial bloom in that incubation (Niraula *et al*, submitted jointly), which appears to have resulted in the larger biomass of bacteria in this incubation. For the 700m case, the best-fit and meidan values of γ_{DiaS} and γ_{DiaL} were higher than their values for the 400m assimilation. However, the best-fit values of both γ_{DiaS} and γ_{DiaL} were low (a few percent or less) in both the 400m and 700m cases (Tables V and VI). Also, the best-fit and median values of γ_{DiaS} were smaller than those of γ_{DiaL} in the 700m assimilation. The problem with the stoichiometry of DOM in the model, together with the problem with the POM data, apparently caused these counter-intuitive values.

In an assimiltion study using data from mesocosm experiments, Vallino (Vallino, 2001), using a model with fixed stoichiometry for phytoplankton, varied the C:N ratio of DOM excretion independently. The best-fit value obtained was quite high (43200:1). Vallino (Vallino, 2001) also reported that including variable stoichiometry of phytoplankton did not improve the model's ability to simulate DOM. In simulations of a station in the English Channel, Anderson and Williams (Anderson and Williams, 1998) tried a model which made DOC production a function of the difference between the light-limited and light-plus-nutrient-limited growth rate of phytoplankton. They compared this to a simpler model in which this excess DOC production was simply proportional to total production and found both lacking. They could not determine which model was better. We tried an assimilation including a similar formulation for excess DOC production, but found only slight improvements in DOM stoichiometry (results not shown). The relatively high standard deviation for DOC measurements, combined with the lack of an upper bound for POM concentrations (discussed above), limited our ability to test different models for DOM formation.

Flows of carbon and nitrogen: The range in the quantiles of simulated net uptake of nitrogen (Figure 9) is narrower than that for gross uptake or gross remineralization. The same is true for carbon (Figure 8). This illustrates that many different values of uptake and remineralization can result in the same net uptake. Still, as discussed above, the stoichiometry of POM constrains nitrogen remineralization, because phytoplankton biomass can only grow with high C:N ratios when DIN supply is limited. The

C:N ratio of phytoplankton in this model is quite sensitive to changes in nitrogen supply, because of the respiration terms that account for the energetic cost of assimilating nitrogen (parameters ζ_A and ζ_N). The more nitrogen phytoplankton assimilate, the more organic carbon they must respire, further lowering their C:N ratio.

The larger spread in the quantiles of simulated net carbon uptake (Figure 8), relative to those for net nitrogen uptake (Figure 9), results partly from variations in the stoichiometry of organic matter. The simulated C:N ratios of POM and DOM vary with phytoplankton stoichiometry and with changes in flows through the ecosystem.

The greater remineralization of nitrogen in the 700m simulations results primarily from the higher values (both best-fit and median) for the rate of bacterial uptake, μ_B, in that assimilation (Tables V and VI, and Figure 3). The remineralization of DON by bacteria in the best-fit simulation of the 700m incubation is approximately twice that in the 400m case (Figures 10 and 11). Production of DON is also slightly greater, because the fractions of production of diatoms (γ_{DiaS} and γ_{DiaL}) are higher in the 700m case (Tables V and VI). However, excretion by phytoplankton was a minor source of DON in both cases.

Microbial versus Grazing Food Web: The cumulative uptake of nitrogen by the MFW increased faster than that for the GFW in the latter half of all three incubations (Figure 12). This trend is consistent with the light-nutrient hypothesis of Elser *et al* (Elser *et al*, 2003), which says that high-light, low-nutrient conditions should favor the MFW.

The MFW dominated uptake of nitrogen in the best-fit simulation and in the quantiles of simulated values for the last two sampling times of each incubation (Figure 12). Uptakes by the MFW and GFW were approximately the same in the first half of the 400m assimilation, but DON concentrations are overestimated in those simulations (Figure 5), meaning that MFW uptake is underestimated for the 400m incubation. Best-fit MFW uptake for the 700m assimilation was approximately 50 % greater than in the 400m case. GFW uptake was also greater in the 700m case, but only by approximately 20 %. Most of the remineralization of nitrogen was mediated by bacteria in both the 400m and 700m simulations.

The increased role of the MFW in the 700m case is consistent with the observation of more DOM and greater bacterial biomass in that incubation. We suspect that differences in phytoplankton assemblages ultimately caused the difference in MFW vs. GFW dominance between the 400m and 700m incubations. Specifically, it appears likely that the dominance of the small diatom *Thalassiosira minima* early in the 700m incubation resulted in the more active MFW. This species is known for copious DOM production. In the simulations, however, differences in excretion of DOM by phytoplankton were

minor (Figures 10 and 11). The higher MFW throughput in the 700m case allowed the GFW uptake to increase as well (Figure 12). This illustrates the ecological role of the MFW, recycling nutrients to keep them available for ecosystems which would otherwise loose them to sinking detritus.

A similar breakdown of MFW vs. GFW uptake for carbon (not shown) reveals smaller differences between the 400m and 700m best-fit simulations. GFW uptake of carbon exceeded MFW uptake by approximately 10 % in the 400m simulations. Uptake of carbon by the MFW and GFW were about the same for the 700m case. These differences between the breakdowns of carbon and nitrogen uptake result from the GFW's higher C:N ratio of uptake relative to the MFW. Also, the lower C:N ratio of phytoplankton biomass in the 700m case compensated for the higher uptake of nitrogen, resulting in only slightly greater total uptake of carbon than in the 400m case (Figure 8).

The simulated flows of carbon and nitrogen are consistent with the lower bulk POC:PON ratio observed towards the end of the 700m incubation, relative to the 400m case. Gross production (or uptake) of both carbon and nitrogen were greater in the 700m case. The difference in nitrogen uptake by large diatoms (dominant in the latter half of both experiments) was greater than the difference in carbon uptake. Thus, the large diatoms grew with lower C:N ratios in the 700m incubation. The higher biomass of bacteria (C:N ratio = 5.1 in this model) in the 700m incubation also contributed directly to the lower bulk POC:PON ratios, but to a lesser extent. The biomass of large diatoms was much greater at the last two sampling times (Figure 6), so their contribution dominated. The lower bulk POC:PON ratio in the 700m incubation results from the greater remineralization of nitrogen by the MFW in that experiment. The link is the flexible composition phytoplankton model.

We have successfully implemented the Monte Carlo Markov Chain method to constrain flows in a complex multi-element ecosystem model. Our ecosystem model, by explicity simulating carbon and nitrogen cycles, was able to consistently simulate the changes in bulk POC:PON ratio over time, and the differences between the incubations using 400m and 700m water. This study has demonstrated that the flexible composition phytoplankton model of Geider *et al* (Geider *et al*, 1998) is well suited for simulating batch incubations of natural seawater. Including this phytoplankton model allowed our assimilation to constrain the remineralization of nitrogen using the observed POM stoichiometry. This was possible despite a problem with the observed amount of POM and the lack of direct measurements of flows through the ecosystem. We were also able to relate the role of the MFW to the bulk stoichiometry of organic matter. Specifically, we found that in the 700m incubation the more active MFW, by regenerating more nitrogen, lowered the C:N ratio of phytoplankton and thereby the bulk POC:PON ratio compared to the 400m case.

Appendix A: Model Description

The model of Geider *et al* (Geider *et al*, 1998), which simulates the C, N and Chl of biomass separately, is applied for each phytoplankton class. Stoichiometries of all other organism-compartments are fixed, and only their nitrogen concentrations are simulated. For each class of non-living organic matter, three elemental fractions are simulated: carbon, nitrogen, and phosphorus. Thus, the stoichiometries of dissolved organic matter (DOM) and particulate organic matter (POM) vary. The elemental fractions of DOM and POM are denoted by DOX and POX, where X (=C, N or P) denotes the elemental fraction.

All other quantities are either terms for processes (defined below) or parameters. Variables for processes are: P_i^{phot} for gross primary production by phytoplankton i; L_i for light-limitation of i; R_x for Respiration by organism x or for Remineralization of compartment x; E_i for Excretion of DOM by phytoplankton i; M_O for Mortality of organism O; $G(i,Z)$ for Grazing of prey i by zooplankton Z; Ege_Z for Egestion of fecal pellets by Z; D_{POX} for dissolution of POX (X = C, N or P) to form DOM; $\Theta_f(T)$ for the temperature dependence of the rate of process f; and RCN_x and RCN_x for the molar C:N and N:P ratio, respectively, of compartment x.

Processes are formulated mostly as in the NEMURO (North pacific Ecosystem Model for Understanding Regional Oceanography) model (Fujii *et al*, 2002a; Eslinger *et al*, 2000), and the carbon and phosphorus cycles are treated as in Smith *et al* (Smith *et al*, 2004). The formulation for bacteria and DOM is based on the model of Anderson and Williams (Anderson and Williams, 1998). Below are the mass balance equations for each compartment.

For $PhyS$ (small, non-silicious phytoplankton), the equation for the C component, $PhyS_C$, is:

$$\frac{\partial PhyS_C}{\partial t} = \{P_{PhyS}^{phot} - R_{PhyS}^C\}PhyS_C - E_{PhyS}^C - \frac{\{M_{PhyS} + G(PhyS,HNF) + G(PhyS,Z)\}}{Q_{PhyS}} \quad \text{(A1)}$$

where P_{PhyS}^{phot} is the gross rate of organic carbon production via photosynthesis, R_{PhyS}^C is the rate of organic C respiration, $-E_{PhyS}^C$ is the rate of excretion of DOC, M_{PhyS} is the rate of mortality (N units), $G(PhyS,HNF)$ is the rate of grazing of $PhyS$ by heterotrophic nanoflagellates (HNF), $G(PhyS,Z)$ is the rate of grazing of $PhyS$ by zooplankton (Z), and Q_{PhyS} is the N:C quota for $PhyS$. For the nitrogen component:

$$\frac{\partial PhyS_N}{\partial t} = \frac{\{V_{C,PhyS}^N - R_{PhyS}^N\}}{Q_{PhyS}}PhyS_N - E_{PhyS}^N$$

$$-\{M_{PhyS}+G(PhyS,HNF)+G(PhyS,Z)\} \tag{A2}$$

where $V^N_{C,PhyS}$ is the rate of uptake of dissolved inorganic nitrogen per mole of C biomass, R^N_{PhyS} is the rate of N respiration, and E^N_{PhyS} is the rate of excretion of *DON*. For the Chl component:

$$\frac{\partial PhyS_{Chl}}{\partial t} = \{\frac{\rho^{Chl}_{PhyS}\cdot V^N_{C,PhyS}}{\Theta^C_{PhyS}} - R^{Chl}_{PhyS}\}PhyS_{Chl} - \frac{\{M_{PhyS}+G(PhyS,HNF)+G(PhyS,Z)\}\Theta^C_{PhyS}}{Q_{PhyS}} \tag{A3}$$

where ρ^{Chl}_{PhyS} is the Chl-synthesis regulating term, R^{Chl}_{PhyS} is the rate of respiration of Chl, and Θ^C_{PhyS} is the ratio of Chl:C for *PhyS*.

Equations for diatoms, *DiaS* and *DiaL* are exactly analogous, except for grazing terms. Heterotrophic nanoflagellates (*HNF*) graze bacteria (*B*) and small phytoplankton (*PhyS*). Zooplankton (*Z*) graze small phytoplankton (*PhyS*), small diatoms (*DiaS*), and heterotrophic nanoflagellates (*HNF*). The model does not include zooplankton large enough to eat the large diatoms, *DiaL*, and so their only loss is mortality. Processes are listed below.

The rate of organic carbon production via photosynthesis, for each phytoplankton class, *i*, is:

$$P^{phot}_i = P^{max}_i \cdot \left(1-\exp\left\{\frac{-\alpha^{Chl}_i\Theta^C_i I}{P^{max}_i}\right\}\right) \tag{A4}$$

in which P^{max}_i is the maximum possible photosynthetic rate:

$$P^{max}_i = P^{ref}_i \cdot \left(\frac{Q_i - Q_{min,i}}{Q_{max,i}-Q_{min,i}}\right)\Theta^{phy}_i(T) \tag{A5}$$

α^{Chl}_i is the Chl-specific light adsorption coefficient, Θ^C_i is the Chl-to-C ratio of phytoplankton *i*, *I* is the light intensity, Q_i is the N:C quota of the phytoplankton, and $Q_{min,i}$ and $Q_{max,i}$ are the minimum and maximum quotas, respectively. Uptake of DIN is:

$$V^N_{C,i} = V^{N,max}_{C,i} f_{upt,i} \tag{A6}$$

where $f_{upt,i}$ is the term for limitation of uptake by external nutrient concentrations:

$$f_{upt,i} = min\left((\frac{NO_3}{K_{NO3,i}\cdot e^{-\Phi_i\cdot NH_4}+NO_3}+\frac{NH_4}{K_{NH4,i}+NH_4}),(\frac{PO_4}{K_{PO4,i}+PO_4})\right) \tag{A7}$$

The maximum possible rate of DIN uptake is:

$$V_{C,i}^{N,max} = v_{C,i}^{N,ref} \Theta_i^{phy}(T) \left[\frac{Q_{max,i} - Q_i}{Q_{max,i} - Q_{min,i}} \right]^{0.05} \quad \text{(A8)}$$

where $v_{C,i}^{N,ref}$ is the maximum possible rate at temperature T_{ref}. The term for Chl-synthesis is:

$$\rho_i^{Chl} = \Theta_i^{N,max} P_i^{phot} / (\alpha_i^{Chl} \Theta_i^C I) \quad \text{(A9)}$$

in which parameter $\Theta_i^{N,max}$ is the maximum possible Chl-to-N ratio for phytoplankton *i*.

As in Geider *et al* (Geider *et al*, 1998), rates of phytoplankton processes depend on temperature:

$$\Theta_i^{phy}(T) = \exp\left(-E_a R_{gas} \cdot \left(\frac{1}{T_{ref}} - \frac{1}{T} \right) \right) \quad \text{(A10)}$$

where E_a is the energy of activation, R_{gas} is the gas constant, and T_{ref} is a reference temperature (at which the rate is specificed). For all other process, *pr*, temperature dependence is expressed as:

$$\Theta_{pr}(T) = \exp\{K_{T,pr} \cdot T\} \quad \text{(A11)}$$

where $K_{T,pr}$ is the parameter for temperature dependence. Respiration of the *C*, *N* and *Chl* in phytoplankton, *i* (= *PhyS*, *DiaS* or *DiaL*), [M nitrogen day^{-1}] is

$$R_i^C = r_i^C \cdot \Theta_{res}(T) \cdot iC - [\zeta_A (1 - f_{new,i}) + \zeta_N f_{new,i}] V_{C,i}^N \quad \text{(A12)}$$

$$R_i^N = r_i^N \cdot \Theta_{res}(T) \cdot iN \quad \text{(A13)}$$

$$R_i^{Chl} = r_i^{Chl} \cdot \Theta_{res}(T) \cdot iChl \quad \text{(A14)}$$

where the r_i's are the parameters for each specific rate of respiration at temperature T_{Ref}, and *iC*, *iN*, and *iChl* are respectively the carbon, nitrogen and Chl concentrations of phytopankton *i*. E_i is Excretion of DON by phytoplankton, *i* [M nitrogen day^{-1}]

$$E_i = \gamma_i \cdot P_i^{phot} \quad \text{(A15)}$$

Mortality of organisms (except bacteria) is [M nitrogen day^{-1}]:

$$M_{Org} = m_{0rg} \cdot \Theta_{mor}(T) \cdot Org^2 \quad \text{(A16)}$$

where m_{Org} is the mortality rate coefficient for each *Org* (= *PhyS*, *DiaS*, *DiaL*, *HNF* or *Z*). Grazing of prey, *p*, by heterotrophs, *h* (= *HNF*, *Z*) [M nitrogen day^{-1}] is:

$$G(p,h) = g_{p2h} \cdot \Theta_{graz}(T) \cdot \ max\Big\{0.0, \quad [1.0 - \exp\{\lambda_I \cdot (p_{min} - p)\}]\Big\} \cdot \ h \tag{A17}$$

in which g_{p2h} is the parameter for maximum grazing rate of *p* by *h* (at 0 $^\circ$ C), and λ_I is the Ivlev coefficient. p_{min} is the minimum concentration for grazing of *p*. The mass balance for heterotrophic nanoflagellates, *HNF*, is:

$$\frac{\partial HNF}{\partial t} = G(B,NHF) + G(PhyS,HNF) - G(NHF,Z) - Ege_{NHF} - R_{NHF} - M_{HNF} \tag{A18}$$

The mass balance for zooplankton, *Z*, is:

$$\frac{\partial Z}{\partial t} = G(NHF,Z) + G(PhyS,Z) + G(DiaS,Z) - Ege_Z - R_Z - M_Z \tag{A19}$$

For each heterotroph, *h* (*h* = *HNF* or *Z*) Ege$_h$ represents egestion of fecal pellets (or DOM for *HNF*) and R_h represents respiration (remineralization), in [M nitrogen day^{-1}].

$$Ege_h = (1 - \alpha_h) \cdot \sum_{p_h} G(p_h,h) \tag{A20}$$

$$R_h = (\alpha_h - \beta_h) \cdot \sum_{p_h} G(p_h,h) \tag{A21}$$

where p_h sums over all prey for *h*. α_h is the assimilation efficiency and β_h is the growth efficiency of *h*. Mortality, M_h, is as defined above.

Mass balances for DIC and nutrients (except silicic acid) follow. Here, sums over *i* count all phytoplankton classes (*i* = *PhyS*, *DiaS* or *DiaL*). Sums over *h* count both *HNF* and *Z*.

$$\frac{\partial DIC}{\partial t} = -\sum_i \{RCN_i \cdot [P_i^{phot} - R_i]\} \quad + \sum_h \{RCN_h^{out} \cdot R_h\} + R_{DOC} + R_{POC} \tag{A22}$$

$$\frac{\partial NH_4}{\partial t} = \sum_i \{R_i - (1 - f_{new,i}) \cdot P_i^{phot}\} + \sum_h \ R_h \quad + R_{DON} + R_{PON} - R_{Nit} \tag{A23}$$

$$\frac{\partial NO_3}{\partial t} = -\sum_i \{f_{new,i} \cdot P_i^{phot}\} \qquad + R_{Nit} \tag{A24}$$

$$\frac{\partial PO_4}{\partial t} = -\sum_i \frac{[P_i^{phot} - R_i]}{RNP_i} + \sum_h \frac{R_h}{RNP_Z^{out}} + R_{DOP} + R_{POP} \quad \text{(A25)}$$

RCN_h^{out} and RNP_h^{out} are the stoichiometric ratios for output from heterotrophic compartment h. These are calculated by mass balance, assuming that the same output stoichiometry applies for both respiration (remineralization) and egestion. both of which are calculated as described above, assuming constant efficiencies for assimilation (α_h) and growth (β_h) on a nitrogen basis.

$$RCN_h^{out} = \frac{\sum_{p_h}[RCN_{p_h} \cdot G(p_h,h)] - \beta_h \cdot RCN_h \cdot \sum_{p_h} G(p_h,h)}{(Ege_h + R_h)} \quad \text{(A26)}$$

$$RNP_h^{out} = \left(Ege_h + R_h\right) \Big/ \left(\sum_{p_h} \frac{G(p_h,h)}{RNP_{p_h}} - \frac{\beta_h}{RNP_h} \cdot \sum_{p_h} G(p_h,h)\right) \quad \text{(A27)}$$

where the sums over p_h count all prey p for each h. $f_{new,i}$ is the fraction of production as NO_3 for each phytoplankton, i (= *PhyS*, *DiaS* or *DiaL*), [dimensionless].

$$f_{new,i} = \frac{\left\{\frac{NO_3}{K_{NO3,i} + NO_3} \cdot e^{-\Phi_i \cdot NH_4}\right\}}{\left\{\frac{NO_3}{K_{NO3,i} + NO_3} \cdot e^{-\Phi_i \cdot NH_4} + \frac{NH_4}{K_{NH4,i} + NH_4}\right\}} \quad \text{(A28)}$$

R_{Nit} is nitrification (oxidation of NH_4 to NO_3) [M nitrogen day^{-1}].

$$R_{Nit} = k_{Nit} \cdot \Theta_{Nit}(T) \cdot NH_4 \quad \text{(A29)}$$

Remineralization of organic matter is R_{DOX} for DOM and R_{POX} for POM, where X (= C, N, or P) represents the elemental fraction. For DOM, these processes depend on bacteria as described below. For POM, remineralization and dissolution, D_{POX}, (to form DOM) are:

$$R_{POX} = k_{r,POM} \cdot \Theta_r(T) \cdot POX \quad \text{(A30)}$$

$$D_{POX} = k_{d,POM} \cdot \Theta_d(T) \cdot POX \quad \text{(A31)}$$

where $k_{r,POM}$ and $k_{d,POM}$ are the rate coefficients for remineralization and dissolution of *POM*. *POM* is produced by mortality (o sums over *DiaS*, *DiaL*, and *Z* below), and by egestion of fecal pellets.

$$\frac{\partial POC}{\partial t} = \sum_o \{RCN_o \cdot M_o\} + RCN_{Zoo}^{out} \cdot Ege_{Zoo} - D_{POC} - R_{POC} \quad \text{(A32)}$$

$$\frac{\partial PON}{\partial t} = \sum_o M_o \qquad + Ege_{Zoo} - D_{PON} - R_{PON} \tag{A33}$$

$$\frac{\partial POP}{\partial t} = \sum_o \{\frac{M_o}{RNP_o}\} \qquad + \frac{Ege_{Zoo}}{RNP^{out}_{Zoo}} - D_{POP} - R_{POP} \tag{A34}$$

Mass balances for dissolved silicic acid and biogenic silica (*BSi*) ollow. *BSi* is produced by mortality of diatoms, and by egestion in fecal pellets by zooplankton (*Z*). Thus *d* sums over *DiaS* and *DiaL* below.

$$\frac{\partial DSi}{\partial t} = -\sum_d \{(P^{phot}_d - R_d - E_d) \cdot RSiN_d\} + R_{BSi} \tag{A35}$$

$$\frac{\partial BSi}{\partial t} = \quad \sum_d \{[M_d + G(d,h)] \cdot RSiN_d\} - R_{BSi} \tag{A36}$$

All *BSi* ingested by zooplankton is assumed to be egested in fecal pellets. Remineralization (dissolution) of *BSi* is expressed as: $R_{BSi} = k_{r,BSi} \cdot \Theta_r(T) \cdot BSi$ [M silicon day^{-1}], where $k_{r,BSi}$ is the rate coefficient. For calcium carbonate, the mass balance is:

$$\frac{\partial CaCO_3}{\partial t} = [M_{PhyS} + G(PhyS,Z)] \cdot RCN_{PhyS} \cdot F_{coc} \cdot RC_{coc} + M_Z \cdot RCN_Z \cdot F_{for} \cdot RC_{for} \quad - R_{cal} \tag{A37}$$

$CaCO_3$ is produced from mortality of *PhyS* and *Z*, and from grazing of calcium carbonate producers. All ingested $CaCO_3$ is assumed to be egested in fecal pellets. RC_{coc} and RC_{for} are the fractions of calcium carbon producers (cocolithophorids and foraminifera, respectively). RC_{coc} and RC_{for} are the ratios of inorganic carbon to organic carbon. R_{cal} is the rate of remineralization (dissolution) of $CaCO_3$ [M Ca day^{-1}]: $R_{cal} = k_{r,cal} \cdot \Theta_r(T) \cdot CaCO_3$.

For bacteria and DOM, the formulation is based on Anderson and Williams (Anderson and Williams, 1998). Their carbon- and nitrogen-based model divided DOM into two classes, labile and semi-labile. We have simplified this to only one class of (non-refractory) DOM by assuming that the labile fraction is consumed instantaneously by bacteria. We use a first-order (in DOM) rate expression. We have also added compartments for the phosphorus fractions of each class of DOM. Refractory DOM is assumed constant.

Uptake of DOM by bacteria is denoted as U_{DOM}. Table III lists parameters for the MFW model. Source/sink terms for each compartment follow. For Bacteria, *B*:

$$\frac{\partial B}{\partial t} = GHP_B - M_B - G(B,HNF) \tag{A38}$$

where GHP_B is the gross heterotrophic procduction (gross growth rate) of bacteria, M_B is their mortality rate, and $G(B,HNF)$ is their rate of grazing by heterotrophic nanoflagellates (*NHF*). The rate of uptake of DOM is based on the carbon fraction, DOC:

$$U_{DOC} = \mu_B \cdot \Theta_r(T) \cdot DOC \cdot B, \tag{A39}$$

in which μ_B is the maximum rate at 0 ° C, $\Theta_r(T)$ is the factor for temperature dependence, and B is the concentration of bacteria. Thus, the rate coefficients, μ_B, have units of [day^{-1} (mole N of bacterial biomass)$^{-1}$]. As in Anderson and Williams (Anderson and Williams, 1998), potential uptake of ammonium and phosphate by bacteria are formulated as Michaelis-Menten type rates:

$$U^{\star}_{NH4} = \frac{\mu_B}{RCN_B} \cdot \Theta_r(T) \cdot \frac{NH_4}{(K_{NH4,B} + NH_4)} \cdot B \tag{A40}$$

$$U^{\star}_{PO4} = \frac{\mu_B}{RCN_B \cdot RNP_B} \cdot \Theta_r(T) \cdot \frac{PO_4}{(K_{PO4,B} + PO_4)} \cdot B \tag{A41}$$

If the total uptake of nutrients (from DOM and inoganic uptake) is sufficient:

$$\frac{\omega_B \cdot U_{DOC}}{RCN_B} < U_{DON} + U^{\star}_{NH3}, \tag{A42}$$

$$\frac{\omega_B \cdot U_{DOC}}{RCN_B \cdot RNP_B} < U_{DOP} + U^{\star}_{PO4}, \tag{A43}$$

and bacteria grow with fixed (carbon-based) growth efficiency, ω_B:

$$GHP_B = \frac{\omega_B \cdot U_{DOC}}{RCN_B} \tag{A44}$$

Remineralization rates for DOM depend on bacteria:

$$R_{DOC} = U_{DOC} - GHP_B \cdot RCN_B \tag{A45}$$

$$R_{DON} = U_{DON} - GHP_B \tag{A46}$$

$$R_{DOP} = U_{DOP} - \frac{GHP_B}{RCN_B \cdot RNP_B} \tag{A47}$$

If either R_{DON} or R_{DOP} is < 0.0, the negative remineralization is the uptake of NH_4 or PO_4 ($U_{NH4} = -R_{DON}$ or $U_{PO4} = -R_{DOP}$), provided the uptake is less than the potential uptake ($-R < U^{\star}$).

If the total uptake of N or P is not sufficient for bacteria to grow with growth efficiency ω_B, $-R_{DON} > U^{\star}_{NH4}$ or $-R_{DOP} > U^{\star}_{PO4}$, the nutrient in shortest supply limits the growth of bacteria. Thus, if $(U_{DOP} + U^{\star}_{PO4}) \cdot RNP_B < (U_{DON} + U^{\star}_{NH4})$, P is limiting, and

$$GHP_B = (U_{DOP} + U^{\star}_{PO4}) \cdot RNP_B \tag{A48}$$

If N is limiting $(U_{DON} + U^{\star}_{NH4}) < (U_{DOP} + U^{\star}_{PO4}) \cdot RNP_B$, and

$$GHP_B = U_{DON} + U^{\star}_{NH_4} \tag{A49}$$

Remineralization is then calculated as above, so that there is no net remineralization of the limiting nutrient. For mortality, M_B, we use the same first-order rate expression as Anderson and Williams (Anderson and Williams, 1998) (with temperature-dependence added):

$$M_B = m_B \cdot \Theta_{mor}(T) \cdot B \tag{A50}$$

in which m_B is the maximum mortality rate coefficient. $G(B,Z)$ is grazing of Bacteria by Z (formulated as the other grazing rates). All bacterial mortality is assumed to become DOM.

The equations for DOM are:

$$\frac{\partial DOC}{\partial t} = \sum_P [RCN_P \cdot E_P] + D_{POC} + RCN_B \cdot M_B - U_{DOC} \tag{A51}$$

$$\frac{\partial DON}{\partial t} = \sum_P E_P + D_{PON} + M_B \quad - U_{DON} \tag{A52}$$

$$\frac{\partial DOP}{\partial t} = \sum_P \frac{E_P}{RNP_P} + D_{POP} + \frac{M_B}{RNP_B} - U_{DOP} \tag{A53}$$

Uptakes of DON and DOP are proportional to the (variable) stoichiometry of DOM. Thus, for U_{DOX}, where X = N or P: $U_{DOX} = (DOX/DOC) \cdot U_{DOC}$.

Acknowledgments. We thank Richard Geider for helpful suggestions about how to embed the phytoplankton model into our ecosystem model. Also, we acknowledege the work of Akari Furuta for the DOM measurements. We thank the staff of the Shizuoka Prefectural Fisheries Laboratory for hosting the experiments and helping with the setup.

References

Anderson, T. R., and P. J. leB. Williams (1998) Modeling the seasonal cycle of dissolved organic carbon at station E1 in the English Channel. *Estuarine Coastal Shelf Sci.*, **46**, 93-109.

Bisset, W. P., J. J. Walsh, D. A. Dieterle and K. L. Carder (1999) Carbon cycling in the upper waters of the Sargasso Sea: I. Numerical simulation of differential carbon and nitrogen fluxes. *Deep-sea Res. I*, **46**, 205-269.

Christian, J. R., M. R. Lewis and D. M. Karl (1997) Vertical fluxes of carbon, nitrogen and phosphorus in the North Pacific Subtropical Gyre near Hawaii. *J. Geophys. Res.*, **102**, C7, 15667–15677.

Elser, J. J., M. Kyle, W. Makino, T. Yoshida and J. Urabe (2003) Ecological stoichiometry in the microbial food web: a test of the light:nutrient hypothesis. *Aquat. Microb. Ecol.*, **31**, 49-65.

Eslinger, D. L., M. Kashiwai, M. J. Kishi, B. A. Megrey, D. M. Ware and F. E. Werner (2000) MODEL Task Team Workshop Report-Final report of the international Workshop to develop a prototype lower trophic level model for comparison of different marine ecosystems in the North pacific. *PICES Scientific report*, No. **15**.

Friedrichs, M. A. M. (2001) Assimilation of JGOFS EqPac and SeaWiFS data into a marine ecosystem model of the Central Equatorial Pacific Ocean. *Deep-sea Res. II*, **49**, 289-319.

Fujii, Masahiko, Y. Nojiri, Y. Yamanaka, and M. J. Kishi (2002a) A one-dimensional ecosystem model applied to time-series Station KNOT. *Deep-Sea Research II*, **49**, 5441-5461.

Fujii, Minoru, S. Murashige, Y. Ohnishi, A. Yuzawa, H. Miyasaka, Y. Suzuki and H. Komiyama (2002b) Decomposition of phytoplankton in seawater. Part 1: Kinetic analysis of the effect of organic matter concentration. *J. Oceanogr.*, **58**, 433–438.

Geider, R. J., H. I. MacIntyre and T. M. Kana (1998) A dynamic regulatory model of phytoplankton acclimation to light, nutrients, and temperature. *Limnol. Oceanogr.*, **43**, 679-694.

Goldman, J. C. and D. A. Caron (1985) Experimental studies on an omnivorous microflagellate: implications for grazing and nutrient regeneration in the marine microbial food chain. *Deep-sea Res.*, **32**, 899-915.

Hargreaves, J. and J. Annan (2002) Assimilation of paleo-data in a simple Earth system model. *Climate Dynamics*, **19**, 371-381.

Harmon, R. and P. Challenor (1997) A Markov chain Monte Carlo method for estimation and assimilation into models. *Ecological Modelling*, **101**, 41-59.

Hood, R. R., N. D. Bates, D. G. Capone, and D. B. Olson (2001) Modeling the effect of nitrogen fixation on carbon and nitrogen fluxes at BATS. *Deep-sea Res. II*, **48**, 1609–1648.

Lefevre, N., A. H. Taylor, F. J. Gilbert and R. J. Geider (2003) Modeling carbon to nitrogen and carbon to chlorophyll a ratios in the ocean at low latitudes: Evaluation of the role of physiological plasticity. *Limnol. Oceanogr.*, **48**, 1796-1807.

Mongin, M., D. M. Nelson, P. Pondaven, M. A. Brzezinski and Paul Treguer (2003) Simulation of upper ocean biogeochemistry with a flexible-composition phytoplankton model: C, N and Si cycling in the western Sargasso Sea. *Deep-sea Res. I*, **50**, 1445-1480.

Schartau, M., A. Oschlies and J. Willebrand (2001) Parameter estimates of a zero-dimensional ecosystem model applying the adjoint method. *Deep-sea Res. II*, **48**, 1769-1800.

Smith, S. L., Y. Yamanaka, and M. J. Kishi (2004) Attempting consistent simulations of Stn. ALOHA with a multi-element ecosystem model. *J. Oceanogr.*, *in press*.

Spitz, Y. H., J. R. Moisan, and M. R. Abbott (2001) Configuring an ecosystem model using data from the Bermuda Atlantic Time Series (BATS). *Deep-sea Res. II*, **48**, 1733-1768.

Vallino, J. J. (2000) Improving marine ecosystem models: use of data assimilation and mesocosm experiments. *J. Marine Res.*, **58**, 117-164.

Verity, P. G. (1991) Measurement and simulation of prey uptake by marine planktonic ciliates fed plastidic and aplastidic nanoplankton. *Limnol. Oceanogr.*, **36**, 729-750.

Figure Captions

Fig. 1: Diagram of the ecosystem model.

Fig. 2: Mass balance of nitrogen for each incubation (using Surface, 400m and 700m water). X's are dissolved inorganic nitrogen (DIN), crosses are (DON + PON), circles are (DIN + DON + PON), and squares are indepently measured TON.

Fig. 3: Top row: evolution of the parameter μ_B (bacterial uptake rate, in day^{-1}) in each of the three assimilations. Horizontal lines are the best-fit values. Bottom row: log of total cost over the course of each of the three assimilations.

Fig. 4: Data (diamonds), best-fit simulation (solid lines) and quantiles of simulated values (dotted lines for 5 %, 50 % and 95 % quantiles) for the Surface incubation. Concentrations (y-axes) are in μM. Symbols for carbon biomasses end in C: BactC (bacteria), DiaSC (small diatoms), DiaLC (large diatoms), HNFC (heterotrophic nanoflagellates), ZooC (zooplankton). LivePOC is the sum of all living biomasses, and others are as defined in the text.

Fig. 5: Data (diamonds), best-fit simulation (solid lines) and quantiles of simulated values (dotted lines for 5 %, 50 % and 95 % quantiles) for the 400m incubation (notation is the same as in Fig. 4). Concentrations (y-axes) are in μM.

Fig. 6: Data (diamonds), best-fit simulation (solid lines) and quantiles of simulated values (dotted lines for 5 %, 50 % and 95 % quantiles) for the 700m incubation (notation is the same as in Fig. 4).

Fig. 7: Observed and simulated POC:PON (bulk) ratios for all three incubations. Dots are data. Solid lines are the best-fit simulation from each assimilation. Dotted lines are the 5 %, 50 % and 95 % quantiles of the simulations.

Fig. 8: Simulated gross production and remineralization of organic carbon and their sum, which is net organic carbon production. Solid lines are from the best-fit simulation, and dotted lines are the 5 %, 50 % and 95 % quantiles of each simulated value. Data points are total organic carbon (TOC = POC + DOC), offset by the observed value at the start of each simulation.

Fig. 9: Simulated gross production and remineralization of organic nitrogen and their sum, which is net organic nitrogen production. Solid lines are from the best-fit simulation, and dotted lines are the 5 %, 50 % and 95 % quantiles of each simulated value. Data points are total organic nitrogen (TON = PON + DON), offset by the observed value at the start of each simulation.

Fig. 10: Cumulative flows of nitrogen in the best-fit simulation of the 400m incubation experiment. Flows (beside arrows) are in μM N. In each compartment's box, the change in its standing stock over the course of the assimilation (final - initial concentration, in μM N) is listed.

Fig. 11: Cumulative flows of nitrogen in the best-fit simulation of the 700m incubation experiment. Notation is the same as in Fig. 10.

Fig. 12: Simulated gross production of organic nitrogen, divided between the Microbial Food Web (MFW) and Grazing Food Web (GFW). Solid lines are from the best-fit simulation, and dotted lines are the 5 %, 50 % and 95 % quantiles of each simulated value.

Table I. Compartments and Variables in the Ecosystem Model

Compartment	Description	Units
	Phytoplankton, $X = C, N, Chl$	
PhySx	Small Phytoplankton	moles x liter^{-1}
DiaSx	Small Diatoms	moles x liter^{-1}
DiaLx	Large Diatoms	moles x liter^{-1}
	Heterotrophs	
B	Bacteria	moles N liter^{-1}
HNF	Heterotrophic Nanoflagellates	moles N liter^{-1}
Z	Zooplankton	moles N liter^{-1}
	Non-living Compartments	
DIC	Dissolved Inorganic Carbon	moles C liter^{-1}
NH_4	Ammonium	moles N liter^{-1}
NO_3	Nitrate	moles N liter^{-1}
PO_4	Phosphate	moles P liter^{-1}
DSi	Silicic acid	moles Si liter^{-1}
BSi	Biogenic Silica (solid)	moles Si liter^{-1}
	Organic Matter, $X = C, N, P$	
DOX	DOM (non-refractory)	moles X liter^{-1}
POX	POM	moles X liter^{-1}
Variable	Description	Units
t	time	seconds
T	Temperature	$^\circ$ C
I	Intensity of Solar Radiation	μmoles photons m^{-2} s^{-1}

Table II. Parameters for phytoplankton

Parameter	value	units	description
i = *PhyS*, *DiaS*, & *DiaL*, indicates a common value for all, otherwise specified separately			
P_i^{ref}	15 *	day^{-1}	max. growth rate at T_{ref} = 20 °C
R_i^C, R_i^N, R_i^{Chl}	0.10	day^{-1}	respiration rates at T_{ref} = 20 °C
α_i^{Chl}	$1 \cdot 10^{-5}$	g C (μmole phot g Chl)$^{-1}$ m^{-2}	Chl-specific light adsorption coeff.
$Q_{min,i}$	0.04	(molar ratio, N:C)	min. cell quota
$Q_{max,i}$	0.20	(molar ratio, N:C)	max. cell quota
$v_{C,i}^{N,ref}$	$Q_{max,i} \cdot P_i^{ref}$	day^{-1}	max. possible DIN uptake rate
$\Theta_{PhyS}^{N,max}$	0.3	g Chl / g N	max. ratio of Chl-to-N for *PhyS*
ζ_N, ζ_A	2.0	mole C / mole N	costs of assimilating NO_3 and NH_4
m_{PhyS}	$5.9 \cdot 10^4$	day^{-1} (mole N liter^{-1})$^{-1}$	mortality rate coefficient at 0 °C
$K_{NO3,PhyS}$	0.5	μM N	half-saturation const., NO_3 uptake
$K_{NH4,PhyS}$	0.1	μM N	half-saturation const., NH_4 uptake
$K_{PO4,PhyS}$	0.00025	μmole P liter^{-1}	half-saturation const., PO_4 uptake
Φ_i	1.5	(μM N)$^{-1}$	*NH4* inhibition of NO_3 uptake
γ_{PhyS}	0.3 *		ratio of excretion : gross production
γ_{DiaS}, γ_{DiaL}	0.1 *		ratio of excretion : gross production
for diatoms, *d* = *DiaS* & *DiaL* (indicating a common value for both)			
$\Theta_d^{N,max}$	0.4	g Chl / g N	max. ratio of Chl-to-N for diatoms
$K_{NO3,d}$	1.0	μM N	half-saturation const., NO_3 uptake
$K_{NH4,d}$	0.10	μM N	half-saturation const., NH_4 uptake
$K_{Si,d}$	1.5	μM N	half-saturation const., *DSi* uptake
$K_{PO4,d}$	0.00125	μM P	half-saturation const., PO_4 uptake
m_d	$2.9 \cdot 10^4$	day^{-1} (mole N liter^{-1})$^{-1}$	mortality rate coefficient at 0 °C

* Parameter varied in the assimilations, using this value as the initial guess.

Table III. Other parameters in the ecosystem model

parameter	value	units	description
		for zooplankton	
RCN_{HNF}, RCN_Z	5.5	(molar ratio, C:N)	fixed stoichiometry of *HNF* and *Z*
g_{p2HNF}, g_{p2Z}	0.5 *	day^{-1}	Grazing rates at 0 °C
α_{HNF}, α_Z	0.7		assimilation efficiency for *HNF* and *Z*
β_{HNF}, β_Z	0.3		rowth efficiency for *HNF* and *Z*
m_{HNF}, m_Z	$5.9 \cdot 10^4$	day^{-1} (mole N $liter^{-1})^{-1}$	mortality rate coefficients at 0 °C
		for bacteria	
RCN_B	5.1	(molar ratio, C:N)	fixed stoichiometry of *B*
μ_B	0.025 *	(μM N $day)^{-1}$	max. uptake rate for DOC at 0 °C
ω_B	0.27		bacterial growth efficiency (C-based)
$K_{NH4,B}$	1.0	μmol N/liter	half-saturation const., NH_4
$K_{PO4,B}$	0.00025	μmol P/liter	half-saturation const., PO_4
m_B	0.02	day^{-1}	bacterial mortality rate coeff. at 0 °C
		others	
RNP_{Org}	16	(molar ratio, N:P)	fixed stoichiometry for all organisms
$RSiN_{DiaS}$, $RSiN_{DiaL}$	1.0	(molar ratio, Si:N)	fixed stoichiometry for all diatoms
$k_{d,POM}$	0.0375	day^{-1}	dissolution rate of POM at 0 °C
$k_{r,POM}$	0.0	day^{-1}	remineralization rate of POM at 0 °C
E_a	$47.3 \cdot 10^3$	Joules $mole^{-1}$	activation energy
$K_{T,pr}$	0.0693	$(°C)^{-1}$	coeff. for temperature dependence

* Parameter varied in the assimilations, using this value as the initial guess.

Table IV. Parameters varied in the assimilation of data from the Surface water incubation

Parameter	initial value	Best	Median	Range	units
for phytoplankton					
P^{ref}_{PhyS}	15.0	13.2	8.09	12.8	day^{-1}
γ_{PhyS}	0.300	0.324	0.505	0.933	[dimensionless]
P^{ref}_{DiaS}	15.0	6.10	8.07	13.2	day^{-1}
γ_{DiaS}	0.100	0.739	0.488	0.867	[dimensionless]
P^{ref}_{DiaL}	15.0	14.1	10.3	8.90	day^{-1}
γ_{DiaL}	0.100	0.589	0.559	0.327	[dimensionless]
for bacteria					
μ_B	0.0250	0.206	1.09	3.14	(μM N day)$^{-1}$
for heterotrophic nanoflagellates and zooplankton					
g_{p2HNF}	0.500	5.90	10.0	8.68	day^{-1}
g_{p2Z}	0.500	4.66	8.05	10.8	day^{-1}
and a perturbations to the initial concentration for each of the six organism classes					

Table V. Parameters varied in the assimilation of data from the 400m water incubation

Parameter	initial value	Best	Median	Range	units
for phytoplankton					
P^{ref}_{PhyS}	15.0	14.0	13.1	5.27	day^{-1}
γ_{PhyS}	0.300	0.0356	0.0472	0.167	[dimensionless]
P^{ref}_{DiaS}	15.0	15.0	14.8	0.644	day^{-1}
γ_{DiaS}	0.100	$8.56 \cdot 10^{-4}$	0.00328	0.0129	[dimensionless]
P^{ref}_{DiaL}	15.0	12.8	13.5	2.25	day^{-1}
γ_{DiaL}	0.100	0.00193	0.00485	0.0192	[dimensionless]
for bacteria					
μ_B	0.0250	0.0608	0.0610	0.0108	(μM N day)$^{-1}$
for heterotrophic nanoflagellates and zooplankton					
g_{p2HNF}	0.500	2.07	2.09	0.171	day^{-1}
g_{p2Z}	0.500	0.661	0.677	0.0662	day^{-1}
and a perturbations to the initial concentration for each of the six organism classes					

Table VI. Parameters varied in the assimilation of data from the 700m water incubation

Parameter	initial value	Best	Median	Range	units
for phytoplankton					
P^{ref}_{PhyS}	15.0	4.69	4.81	11.4	day^{-1}
γ_{PhyS}	0.300	0.443	0.310	0.492	[dimensionless]
P^{ref}_{DiaS}	15.0	15.0	14.7	1.21	day^{-1}
γ_{DiaS}	0.100	0.0121	0.0102	0.0343	[dimensionless]
P^{ref}_{DiaL}	15.0	9.78	10.3	1.42	day^{-1}
γ_{DiaL}	0.100	0.0181	0.0201	0.0668	[dimensionless]
for bacteria					
μ_B	0.0250	0.0824	0.0827	0.0182	(μM N day)$^{-1}$
for heterotrophic nanoflagellates and zooplankton					
g_{p2HNF}	0.500	2.31	2.20	0.251	day^{-1}
g_{p2Z}	0.500	0.624	0.606	0.0405	day^{-1}
and a perturbations to the initial concentration for each of the six organism classes					

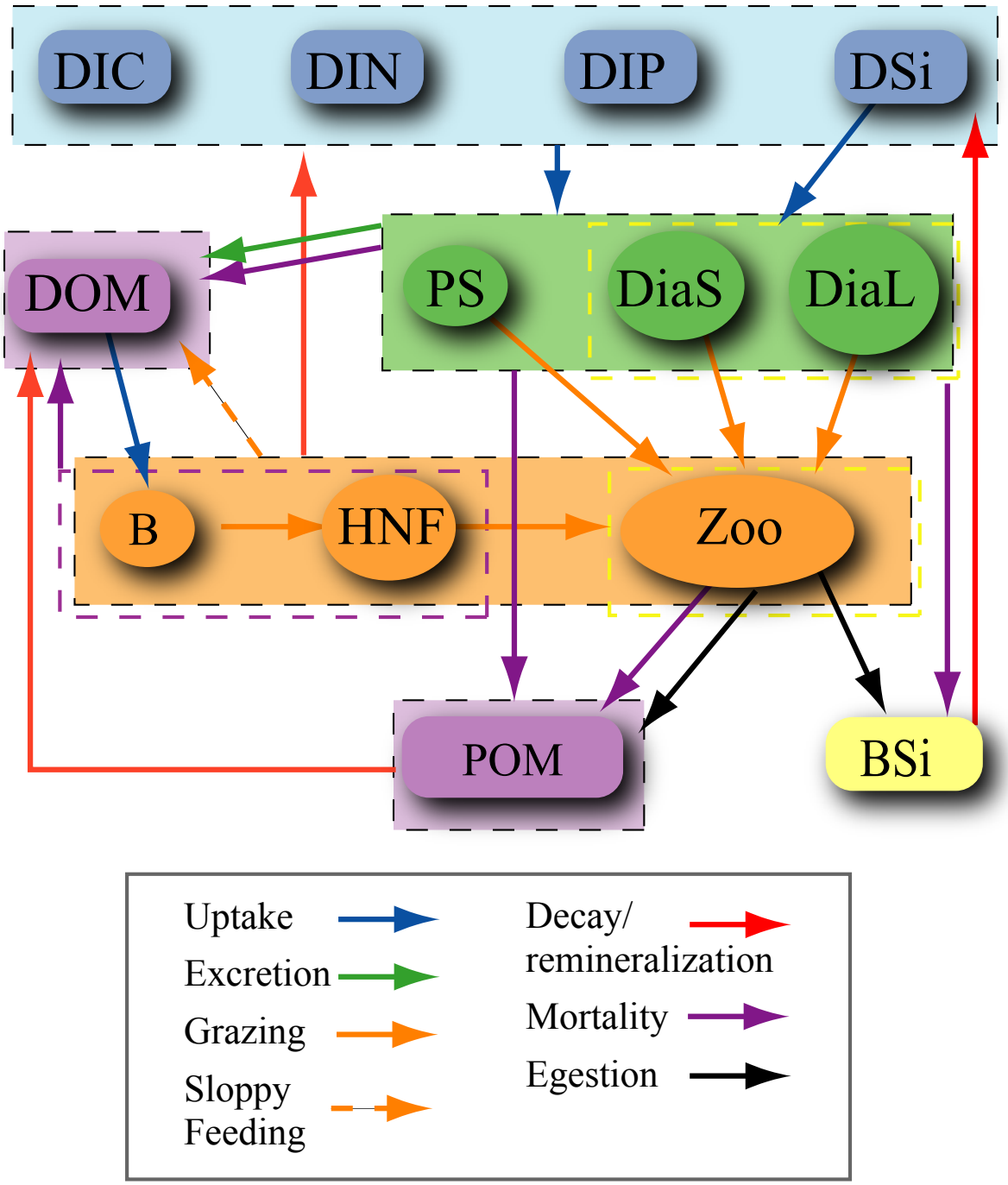
DIC
DIN
DIP
DSi
DOM
PS
DiaS
DiaL
B
HNF
Zoo
POM
BSi
Uptake
Excretion
Grazing
Sloppy Feeding
Decay/ remineralization
Mortality
Egestion

Figure 1.

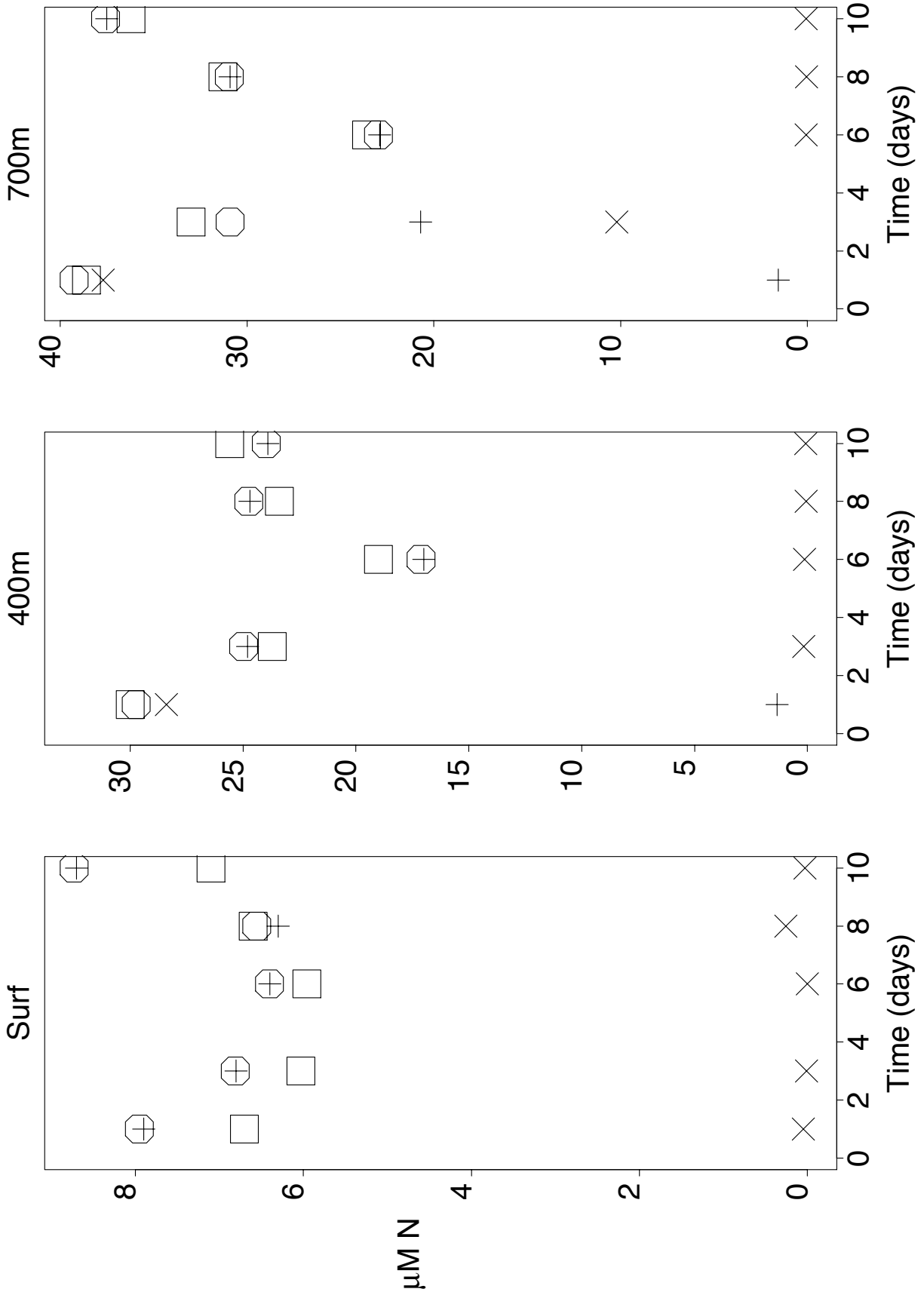

Figure 2.

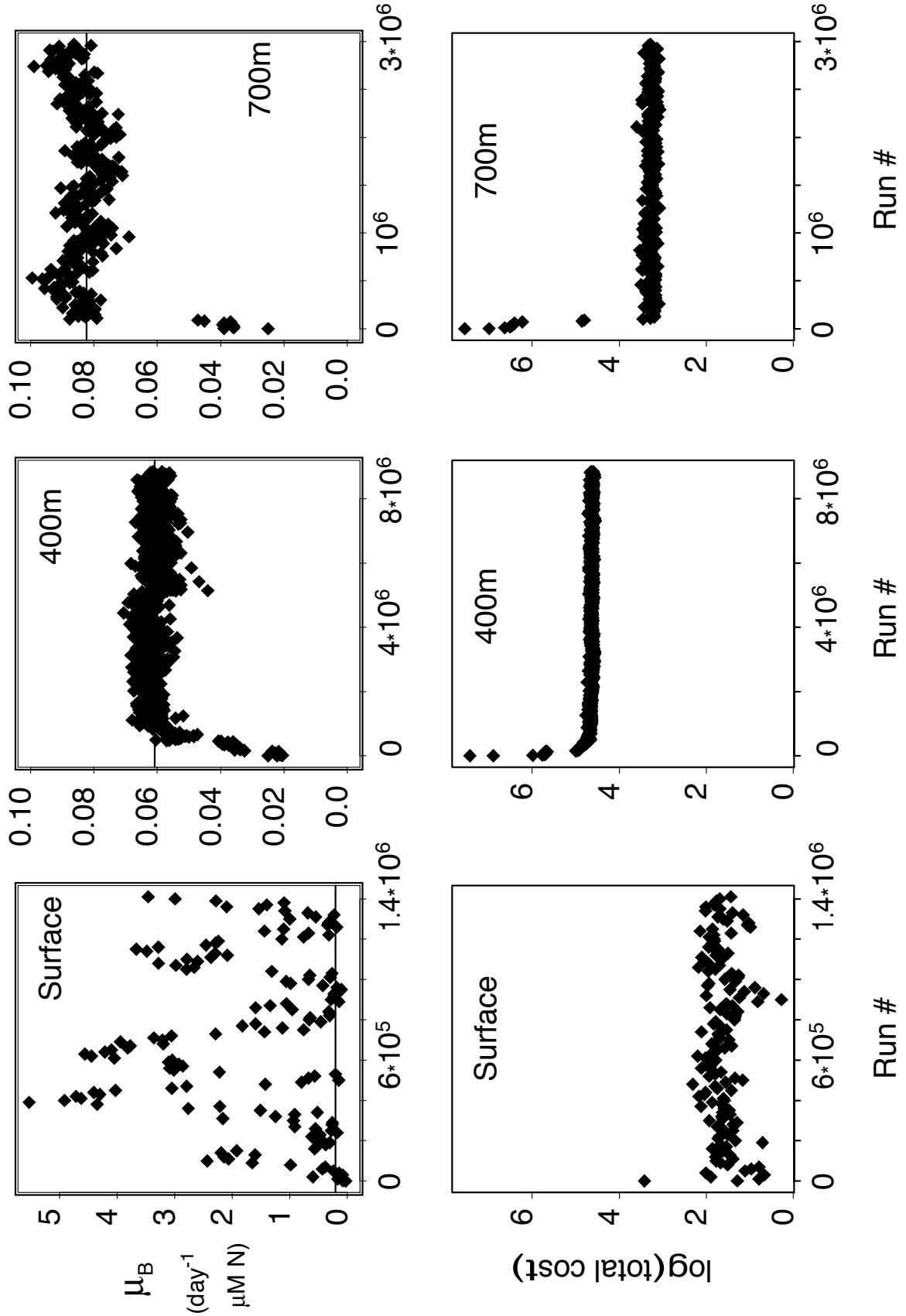
Surface
400m
700m
μ_B (day^{-1} μM N)
log(total cost)
Run #
0
6*10^5
1.4*10^6
4*10^6
8*10^6
10^6
3*10^6
0.0
0.02
0.04
0.06
0.08
0.10
2
4
6

Figure 3.

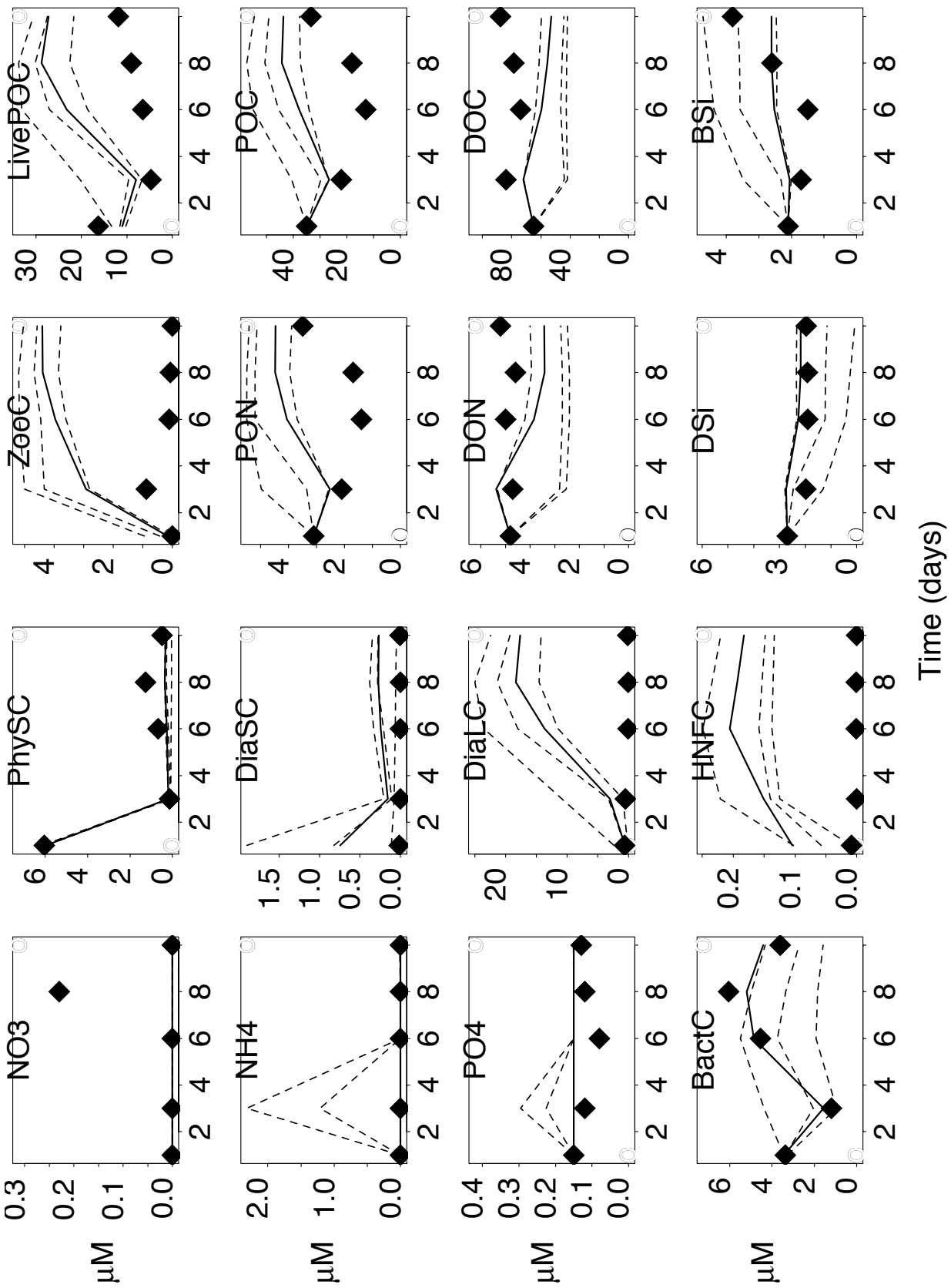
NO3
PhySC
ZooC
LivePOC
NH4
DiaSC
PON
POC
PO4
DiaLC
DON
DOC
BactC
HNFC
DSi
BSi
µM
Time (days)

Figure 4.

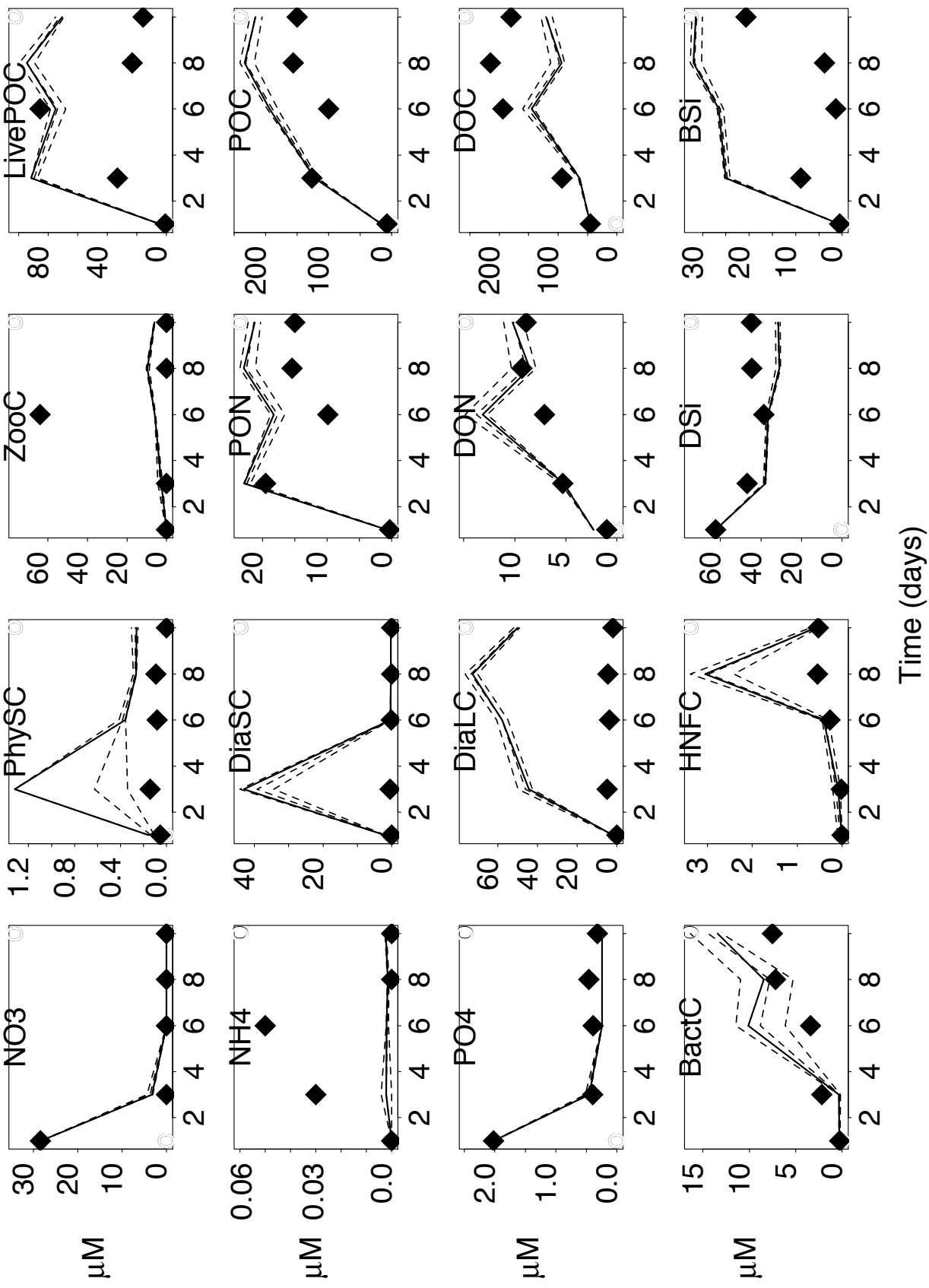
NO3
PhySC
ZooC
LivePOC
NH4
DiaSC
PON
POC
PO4
DiaLC
DON
DOC
BactC
HNFC
DSi
BSi
µM
Time (days)

Figure 5.

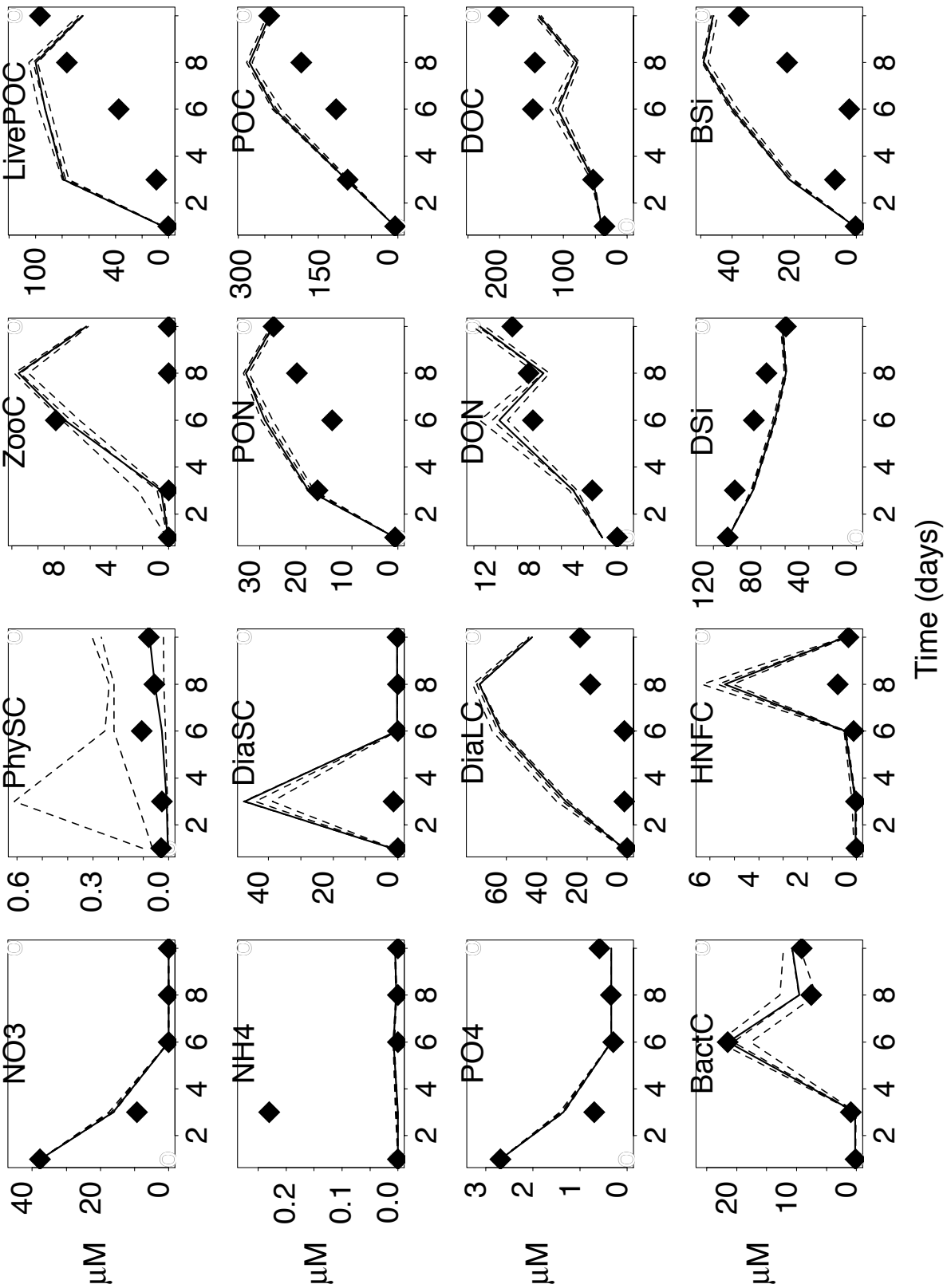
NO3
NH4
PO4
BactC
PhySC
DiaSC
DiaLC
HNFC
ZooC
PON
DON
DSi
LivePOC
POC
DOC
BSi
μM
Time (days)

Figure 6.

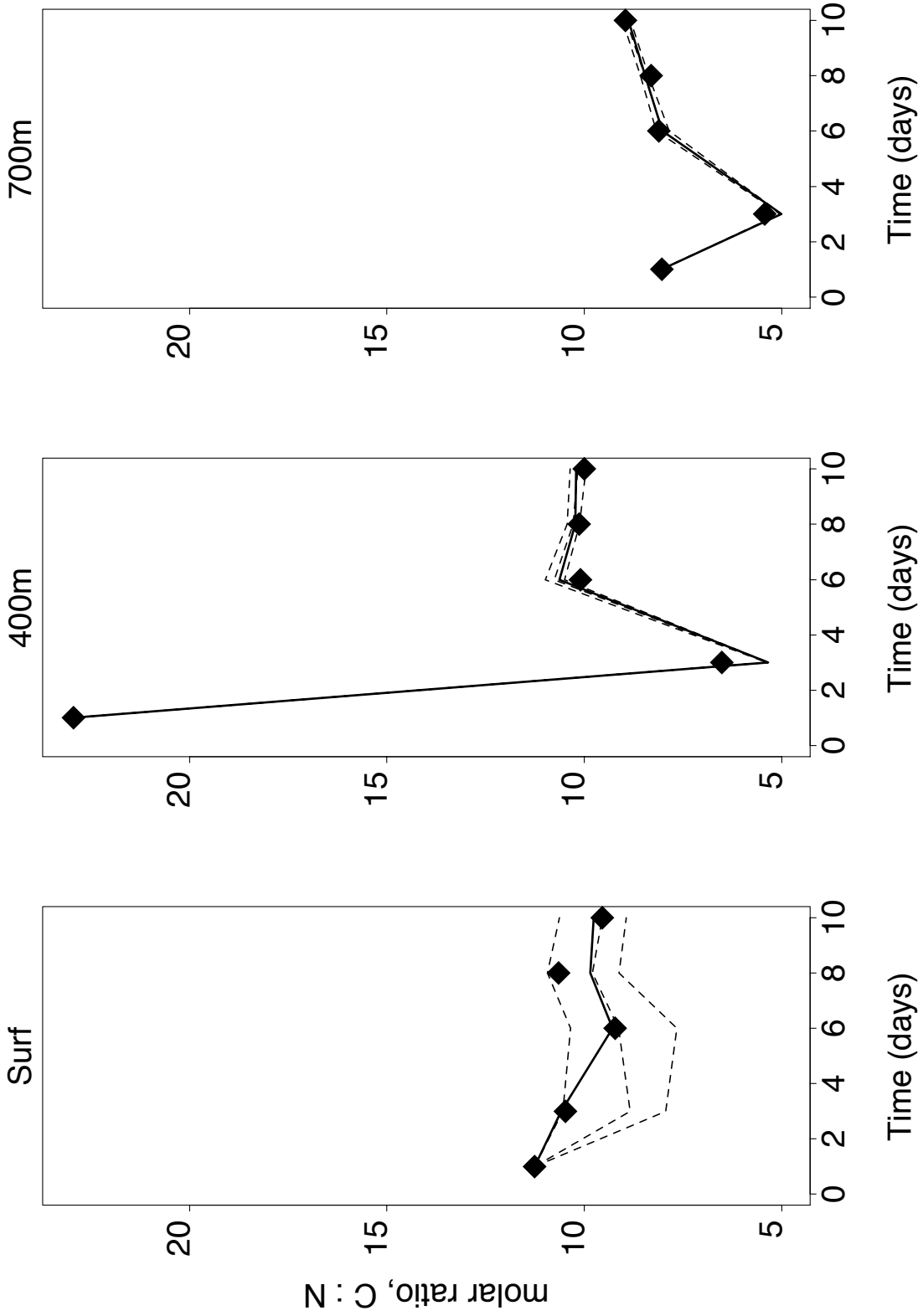

Figure 7.

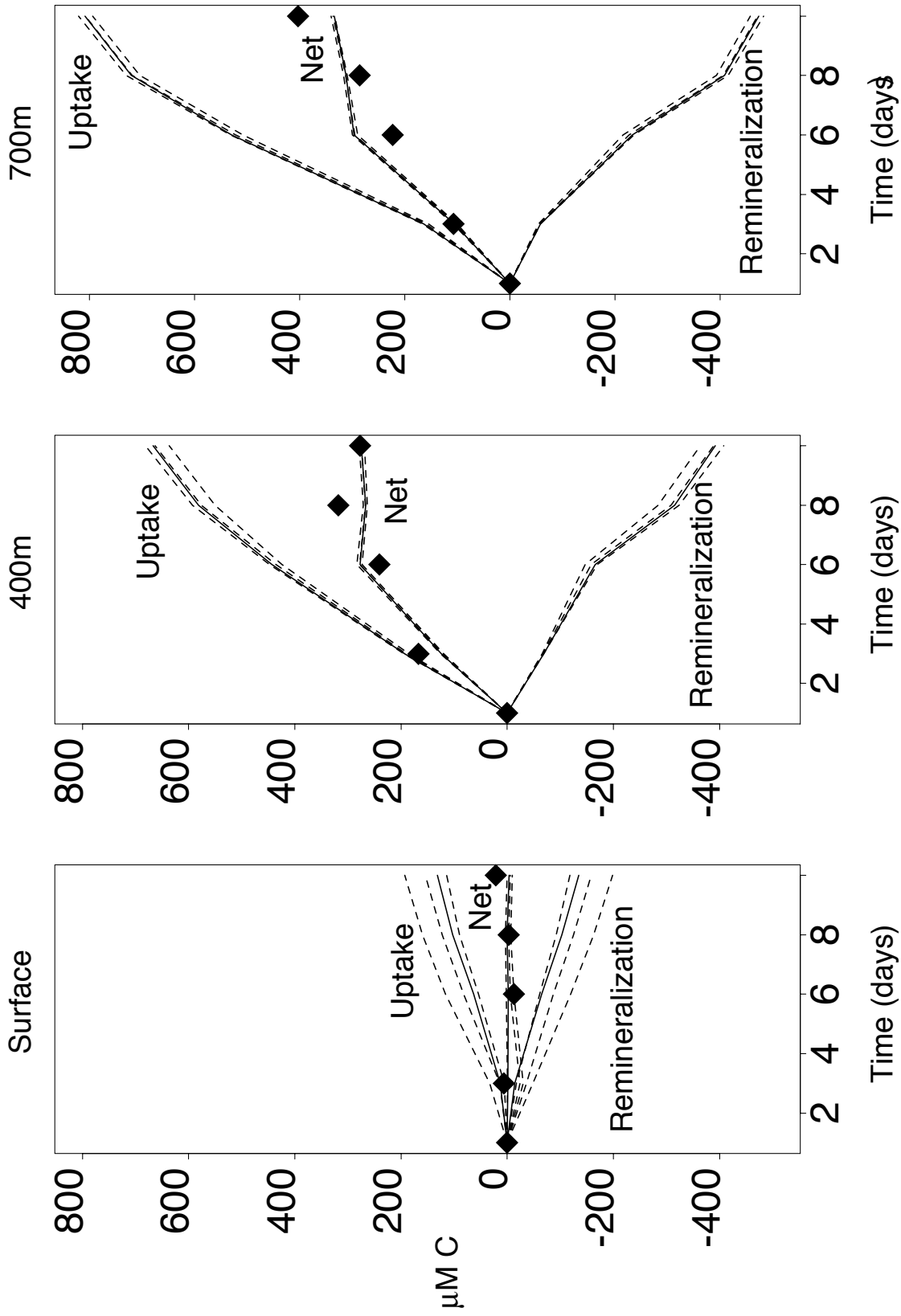
700m
400m
Surface
Uptake
Net
Remineralization
Time (days)
800
600
400
200
0
-200
-400
2 4 6 8
µM C

Figure 8.

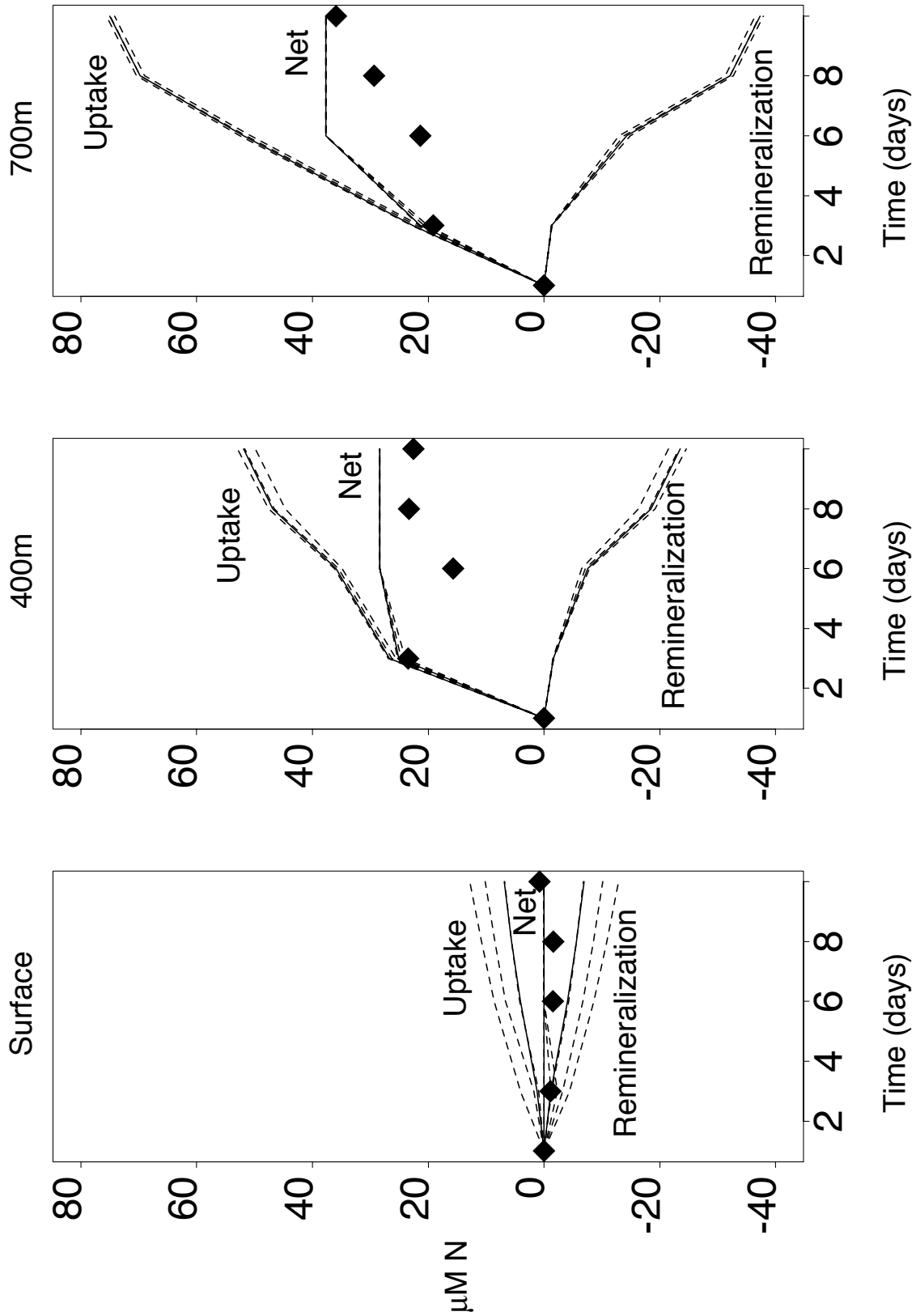
700m
400m
Surface
Uptake
Net
Remineralization
Time (days)
μM N
80
60
40
20
0
-20
-40
2
4
6
8

Figure 9.

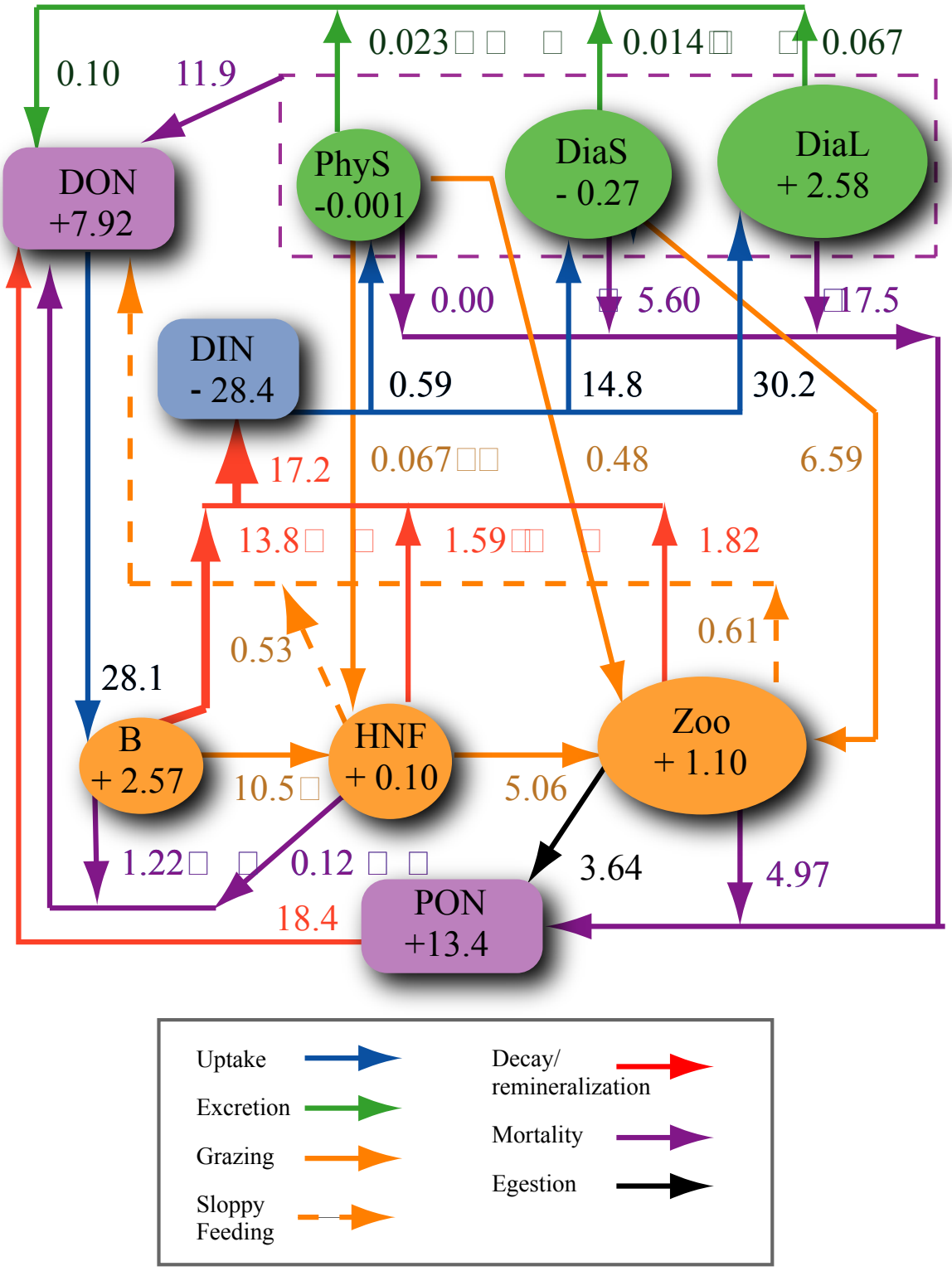
0.10
11.9
0.023
0.014
0.067
DON
+7.92
PhyS
-0.001
DiaS
- 0.27
DiaL
+ 2.58
0.00
5.60
17.5
DIN
- 28.4
0.59
14.8
30.2
17.2
0.067
0.48
6.59
13.8
1.59
1.82
0.53
0.61
28.1
B
+ 2.57
HNF
+ 0.10
Zoo
+ 1.10
10.5
5.06
1.22
0.12
3.64
4.97
18.4
PON
+13.4
Uptake
Excretion
Grazing
Sloppy Feeding
Decay/ remineralization
Mortality
Egestion

Figure 10.

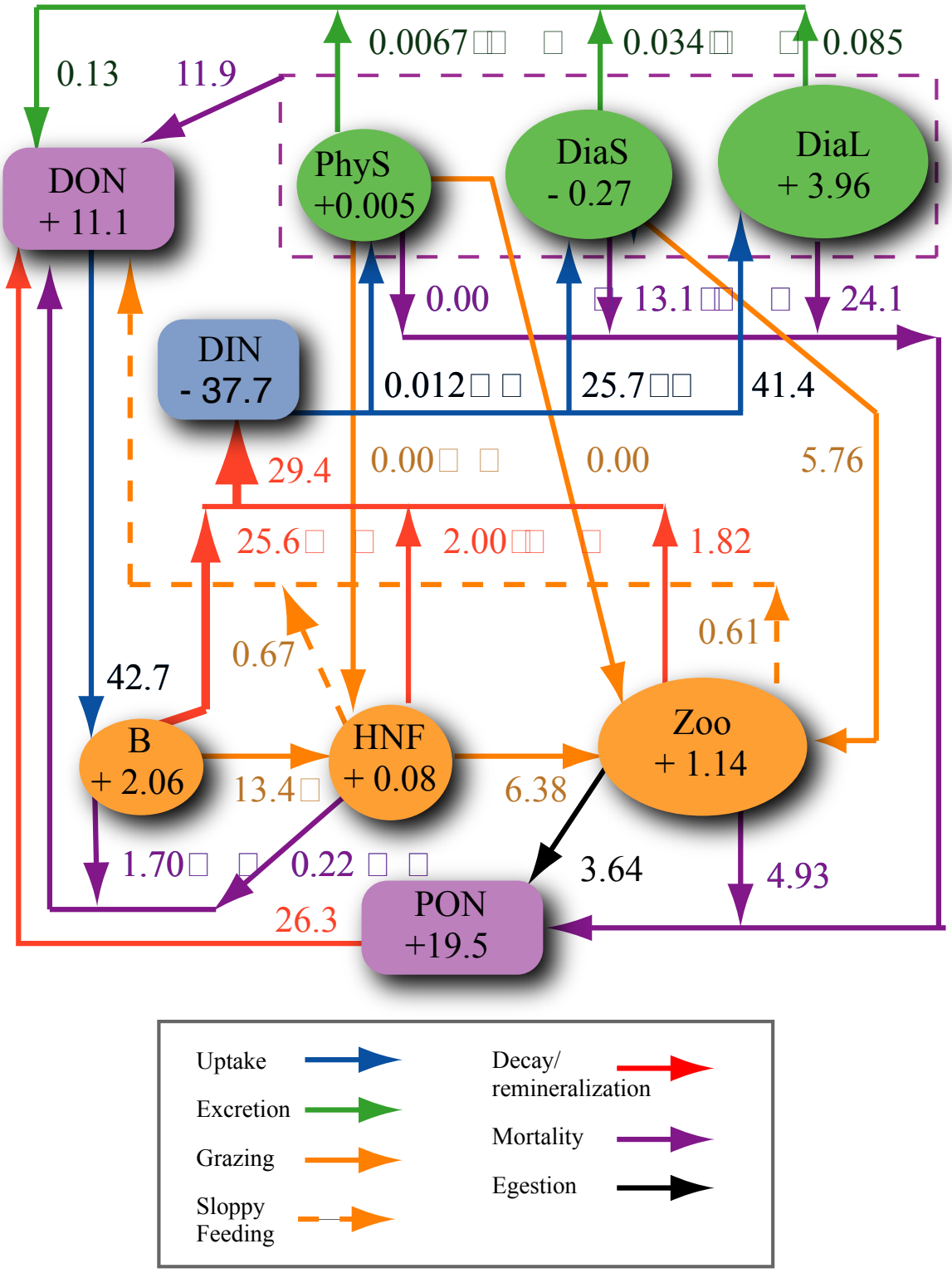
0.13
11.9
0.0067
0.034
0.085
DON
+ 11.1
PhyS
+0.005
DiaS
- 0.27
DiaL
+ 3.96
0.00
13.1
24.1
DIN
- 37.7
0.012
25.7
41.4
29.4
0.00
0.00
5.76
25.6
2.00
1.82
0.67
0.61
42.7
B
+ 2.06
HNF
+ 0.08
Zoo
+ 1.14
13.4
6.38
1.70
0.22
3.64
4.93
26.3
PON
+19.5
Uptake
Excretion
Grazing
Sloppy Feeding
Decay/ remineralization
Mortality
Egestion

Figure 11.

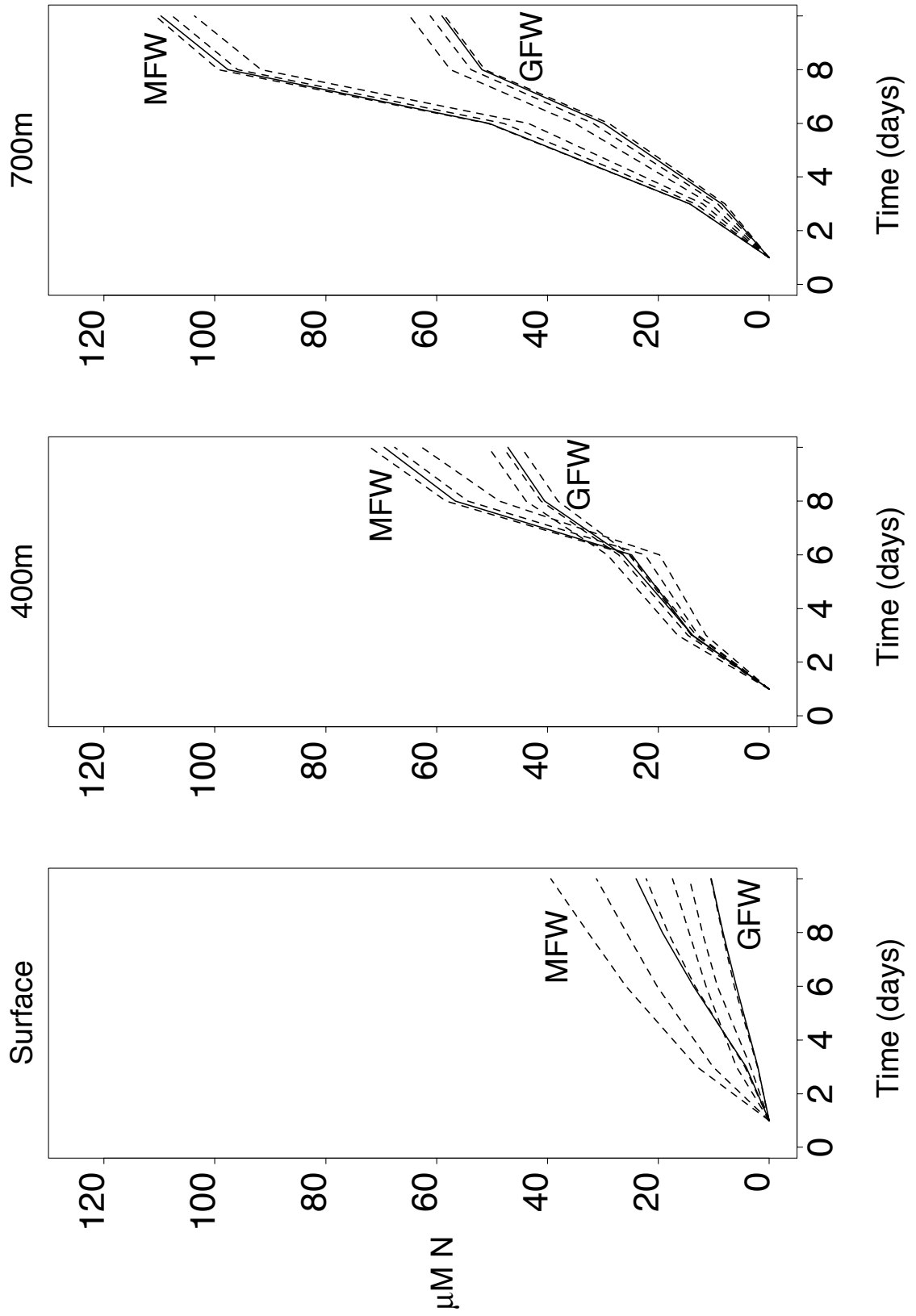
700m
400m
Surface
MFW
GFW
μM N
Time (days)
0
20
40
60
80
100
120
0
2
4
6
8

Figure 12.